

EPA-650/2-73-045

December 1973

Environmental Protection Technology Series

# **A STUDY OF COMBUSTOR FLOW COMPUTATIONS AND COMPARISON WITH EXPERIMENT**



Office of Research and Development  
U.S. Environmental Protection Agency  
Washington, D.C. 20460

# **A STUDY OF COMBUSTOR FLOW COMPUTATIONS AND COMPARISON WITH EXPERIMENT**

by

R. F. Anasoulis and H. McDonald

United Aircraft Research Laboratories  
400 Main Street  
East Hartford, Connecticut 06108

Contract No. 68-02-0267  
Program Element No. 1AB014  
ROAP No. 21ADG-10

EPA Project Officer: D. W. Pershing

Control Systems Laboratory  
National Environmental Research Center  
Research Triangle Park, North Carolina 27711

Prepared for

OFFICE OF RESEARCH AND DEVELOPMENT  
U.S. ENVIRONMENTAL PROTECTION AGENCY  
WASHINGTON, D.C. 20460

December 1973

**This report has been reviewed by the Environmental Protection Agency and approved for publication. Approval does not signify that the contents necessarily reflect the views and policies of the Agency, nor does mention of trade names or commercial products constitute endorsement or recommendation for use.**



## ABSTRACT

A computational procedure for calculating the coupled flow and chemistry within combustion devices is presented. The procedure solves the time-averaged Navier-Stokes equations with coupled chemistry, including the effects of turbulence and radiative heat transfer, using a novel field relaxation method developed at the United Aircraft Research Laboratories. Although a relatively simple turbulence model is employed in the procedure, modification to this model is easily implemented within the framework of the computational method. Computations of the flow and chemistry within a representative furnace have been made using the procedure and are presented and compared with experimental data.

This report was submitted in fulfillment of Contract 68-02-0267 by United Aircraft Research Laboratories, under the sponsorship of the Environmental Protection Agency. Work was completed as of December 1973.

## CONTENTS

	<u>Page</u>
ABSTRACT. . . . .	iii
LIST OF FIGURES . . . . .	vi
LIST OF TABLES. . . . .	viii
ACKNOWLEDGMENTS . . . . .	ix

### SECTION

I	INTRODUCTION . . . . .	1
II	THEORETICAL ANALYSIS.. . . .	4
III	COMPUTATIONAL ANALYSIS . . . . .	33
IV	RESULTS AND DISCUSSION . . . . .	56
V	CONCLUSIONS. . . . .	78
VI	REFERENCES . . . . .	80
VII	LIST OF SYMBOLS. . . . .	85

## FIGURES

<u>No.</u>		<u>Page</u>
1	Coordinate System for Radiant Flux. . . . .	22
2	Burner Flow Model . . . . .	28
3	Relaxation Procedures . . . . .	35
4	Vorticity Residual History. . . . .	36
5	Vorticity Residual History. . . . .	38
6	Computed Velocity Distributions . . . . .	39
7	Extrapolation Procedure . . . . .	45
8	A Comparison Between Predicted and Measured Axial Decay of The Velocity Maximum in a Turbulent Swirling Jet. . . . .	60
9	A Comparison Between Predicted and Measured Axial Decay of The Swirl Velocity Maximum in a Turbulent Swirling Jet. . . . .	61
10	Comparison Between Theory and Measurement of the Mean Velocity Profile in a Turbulent Swirling Jet . . . . .	62
11	A Comparison Between Predicted and Measured Axial Decay of The Velocity Maximum in a Turbulent Swirling Jet. . . . .	63
12	A Comparison Between Predicted and Measured Axial Decay of The Swirl Velocity Maximum in a Turbulent Swirling Jet. . . . .	64
13	The Comparison Between Theory and Measurement of the Mean Velocity Profile in a Turbulent Swirling Jet. . . . .	65
14	A Comparison Between Predicted and Measured Axial Decay of The Velocity Maximum in a Turbulent Swirling Jet. . . . .	66
15	A Comparison Between Predicted and Measured Axial Decay of The Swirl Velocity Maximum in a Turbulent Swirling Jet. . . . .	67

## FIGURES (Concluded)

<u>No.</u>		<u>Page</u>
16	Comparison Between Theory and Measurement of the Mean Velocity Profile in a Turbulent Swirling Jet. . . . .	68
17	Radial Distribution of Velocity Vector. . . . .	69
18	Radial Distribution of the Axial Velocity . . . . .	70
19	Radial Distribution of Axial Velocity . . . . .	71
20	Theoretical Streamlines for IGT Swirl Burner. . . . .	72

# TABLES

<u>No.</u>		<u>Page</u>
I	Coefficients of General Elliptic Equation. . . . .	8
II	Chemical Rate Constants. . . . .	17
III	Auxiliary Reactions for Hydrocarbon Combustion Equilibrium Model. . . . .	20



## ACKNOWLEDGMENTS

Dr. W. R. Briley contributed greatly to the successful development of the FREP code described in the present report. In addition, Mr. W. A. Carey constructed the code input/output procedures, including the overlay and peripheral storage routines while Mr. R. C. Buggeln gave considerable assistance with the running of the test cases. The work was supported by the Environmental Protection Agency under Contract No. 68-02-0267 with Mr. David Pershing as the Contract Officer.

## SECTION I

### INTRODUCTION

Concern over air pollution and increased demands for higher efficiency have placed considerable burden on present day designers of furnaces. Methods for modeling furnaces have generally been less than completely satisfactory largely due to lack of understanding of the fundamental flow processes which, through heat, mass, and momentum exchange, directly influence pollutant emission generation and combustion efficiency. For example, it has been shown (Refs. 1 and 2) that stability and combustion intensity of flames as well as residence time in furnaces are strongly influenced by swirling flow. Residence times and flame stability and intensity are, in turn, related to furnace performance and efficiency as well as to pollutant emission formation (Refs. 3 and 4). Thus, because of the strong influence of flow processes on combustion characteristics, it is particularly important that the fluid mechanics be properly taken into account in development of furnace modeling techniques.

Procedures employed for modeling combustion processes have generally been highly simplified, particularly in regard to flow modeling where stirred reactor concepts and one-dimensional assumptions are employed (Refs. 5 through 10). Examples are the studies conducted by Fletcher and Heywood (Ref. 5) and Hammond and Mellor (Refs. 6 and 7), who employed the stirred reactor concept to model the flow in the primary zone of gas turbine combustion chambers in order to assess the effect of residence time on combustion behavior and to predict pollutant emissions. Although radiant heat transport was neglected in both these studies, a sophisticated chemistry model, based on quasi-global finite-rate hydrocarbon mechanism, was employed by Hammond and Mellor to account for the fuel decomposition. Other studies included the analysis of Roberts, et al., (Ref. 8), who, in order to predict nitric oxide production in gas turbine combustors, divided the combustion chamber into three regions: one corresponding to the central recirculation portion of the upstream zone; a second representing the flow region surrounding the recirculation zone which was interpreted to be a one-dimensional reacting zone; and the third downstream zone modeled as a one-dimensional region. An interesting result of the Roberts analysis was the small difference noted in predicted nitric oxide levels in comparisons between coupled and uncoupled hydrocarbon thermochemistry systems which were studied; thereby, suggesting that a decoupling of the hydrocarbon chemistry from the nitric oxide chemistry might be a reasonable approximation. No account was taken of radiant heat transport in the Roberts analysis. An extension of the Roberts, et al., analysis, directed toward low power gas turbine operation, was developed by

Mosier, et al., (Ref. 9), where, by employing a more sophisticated finite-rate hydrocarbon mechanism, trends were predicted which were in agreement with experimental data. In another study, Edelman and Economos (Ref. 10), in an attempt at developing a general analytical procedure for predicting combustion behavior, applied a modular technique whereby various critical combustion processes were treated on an individual basis or coupled as a function of operating conditions. The Edelman approach may be criticized in its manner of accounting for recirculation (a stirred reaction is used), disregard of radiative transport effects, and its inability to provide a unified description of a combustion chamber under a given set of operating conditions.

As a general criticism, it seems that all of the foregoing methods are lacking primarily in their ability to properly account for mixing and reverse flow phenomena occurring in the recirculation zone of a furnace. However, a computational method which does allow for calculation in recirculation regions has been proposed recently by Gosman, et al., (Ref. 11), who solved the governing equations by a relatively inefficient explicit point by point relaxation procedure. Employing the Gosman method to demonstrate the feasibility of making computations in the recirculation zones of combustion chambers, sample computations were conducted at UARL in a representative burner (Ref. 12). Highly simplified chemistry and turbulence models were employed in these initial predictions but no account was taken of radiative transport. The results obtained with this procedure demonstrated qualitative agreement with experimental observations, and were very encouraging and, as a consequence, led to development by UARL of an improved numerical code for solving combustng flows containing recirculation zones. The UARL procedure is a novel implicit computational scheme in which residuals are relaxed simultaneously throughout the entire flow field rather than one at a time which is characteristic of the explicit point methods. Because of this feature the UARL code has proven to be considerably more efficient than the point methods, especially as the number of grid nodes are increased.

A principal objective of the study under this contract was to further develop and refine the UARL computational procedure in order to determine and demonstrate the potential for predicting air pollutant emissions from furnaces. For this purpose, computations of the flow field within a representative furnace were undertaken as part of this contract and comparisons made against both hot- and cold-flow measurements. The computational procedure, which is referred to as the FREP code (acronym for Field Relaxation Elliptic Procedure), solves the time-averaged Navier-Stokes equations with coupled chemistry, turbulence, and radiant heat transfer models. The turbulence model consists of an eddy viscosity model derived from an extension of Prandtl's mixing length hypothesis and a wall-flux model which is employed

to resolve the flow field in the immediate vicinity of the wall where large gradients are known to exist. (The turbulence model was partially developed under a jointly sponsored FAA/WPAFB-APL contract, No. F33615-72-C-2042.) The radiant heat transfer model incorporated into the procedure is a four-flux collimated model requiring solution of two differential equations to obtain the flux of radiant energy in the radial and axial directions. The radiant heat flux obtained by solution of these equations is included as an additional term in the energy equation. The chemistry model is based on equilibrium hydrocarbon chemistry coupled with finite-rate nitric oxide chemistry. The intent in development of the flow models, described above, was to minimize undue complexity and sophistication and to provide a reasonably good framework within which refinements could be easily implemented at a future time, if warranted by comparison with experimental data.

## SECTION II

### THEORETICAL ANALYSIS

#### II-A. APPROACH

The flow regime considered in the present study is a quasi-steady gaseous phase turbulent flow system with combustion. Turbulent exchange coefficients, defined by analogy with Newton's, Fourier's, and Fick's laws for laminar flows, are employed to define momentum, enthalpy, and chemical species fluxes, respectively. A knowledge of these turbulent fluxes is required to close the governing system of equations. Values for the exchange coefficients are determined by specification of a turbulence model together with values of Prandtl and Schmidt numbers taken from knowledge of turbulent flows of gases and gas mixtures. A chemistry model and a radiation model are employed to evaluate chemical species rate expressions and radiation heat transfer effects on furnace characteristics.

In order to solve the combustion problem, it is necessary, in addition to specifying turbulent transport models, to employ a computational method for solving the complex system of equations. The computational procedure must be capable of treating the flow resulting from the interaction of mixing and chemical reactions in the turbulent diffusion flame and from sudden changes in flow properties which may be prompted as a result of the combustion process, any or all of which could lead to eventual divergent behavior. Taking into consideration these potential difficulties, a powerful novel numerical procedure, developed at UARL, is applied under this contract to the solution of the equations governing the flow and chemistry within a representative furnace. Time-mean-average velocities, pressure, temperatures, and concentrations are computed and comparisons are made against measurements to allow for an evaluation of the procedure and possible improvements in hypotheses and in furnace analytical modeling techniques.

#### II-B. GOVERNING EQUATIONS

Under consideration is the flow of a turbulent radiating chemically reacting multicomponent mixture with heat and mass transport. The elliptic time-averaged partial differential equations describing this combustion system are based on the conservation laws of mass, momentum, energy, and chemical species (Ref. 13). For simplicity, these equations are expressed in vector notation below. Negligible coupling between diffusion and thermal gradients, no body forces, and negligible bulk viscosity all are assumed. Fick's law is

presumed valid throughout, implying equal binary diffusion coefficients for each pair of species in the mixture. The resulting set of equations can be written

Continuity:

$$\nabla \cdot \rho \mathbf{v} = 0 \quad (1)$$

Conservation of Species:

$$\nabla \cdot \rho \mathbf{v} m_i - \nabla \cdot \left( \sum_j \Gamma_{ij} \nabla m_j \right) - r_i - \sum_j r_{ij} = 0 \quad (2)$$

Conservation of Momentum:

$$\nabla \cdot \rho \mathbf{v} \mathbf{v} - \mu_{\text{eff}} \left[ \nabla \mathbf{v} + \nabla \mathbf{v}^T - \frac{2}{3} (\nabla \cdot \mathbf{v}) \delta \right] + \nabla P = 0 \quad (3)$$

Conservation of Energy:

$$\nabla \cdot \rho \mathbf{v} H - \nabla \cdot \left( \sum_i \Gamma_i h_i \nabla m_i \right) - \nabla \cdot (\Gamma_h C_p \nabla T) - \nabla \cdot (\mu_{\text{eff}} \nabla (v^2/2)) + Q_R = 0 \quad (4)$$

There is also the thermodynamic relationships

$$P = \frac{\rho R T}{M} \quad (5)$$

$$H = \int \left( \sum_i C_{p,i} m_i \right) dT + \sum_i h_i m_i + \frac{v^2}{2} \quad (6)$$

which provide additional equations necessary to close the system. These equations are written for variable fluid properties and embody mass diffusion, chemical reaction, radiation heat transfer, and viscous dissipation. In the energy equation, the kinetic heating terms, which assume importance only when the swirl component of velocity predominates, have been neglected. In order to solve the above equations in addition to boundary conditions, it is necessary to specify expressions for turbulent exchange coefficients,  $\Gamma_i$ ,  $\Gamma_h$ , and  $\mu_{eff}$ , rate of generation of chemical species,  $r_i$  (in this case only nitric oxide), and radiant energy transport,  $Q_r$ . In regard to the turbulent exchange coefficients, because in the present analysis Prandtl and Schmidt numbers are employed in the computations based on knowledge of turbulent flows of gases and gas mixtures, only a turbulent momentum exchange coefficient (i.e.,  $\mu_{eff}$ ) need be specified. This is a consequence of the fact that the enthalpy and chemical species turbulent exchange coefficients are related to the turbulent effective Prandtl and Schmidt numbers through the effective viscosity via the relations

$$Pr_{eff} = \frac{\mu_{eff}}{\Gamma_h} \quad (7)$$

$$Sc_{eff} = \frac{\mu_{eff}}{\Gamma_i} \quad (8)$$

To define the effective viscosity,  $\mu_{eff}$ , a turbulence model is employed. Likewise, a chemistry model and a radiation model are employed to define the rate of production of chemical species and radiant energy transports, respectively. These models are discussed in detail in subsequent sections. At this time it is convenient to express the momentum equations in alternate form in terms of vorticity and stream function. This is done in order to make the subsequent mathematical treatment easier to follow and because it is more convenient in the numerical computational procedure since it eliminates pressure as a variable.

For the axisymmetric case, vorticity and stream function can be defined in cylindrical coordinates according to the following relations:



$$\omega = \frac{\partial v}{\partial x} - \frac{\partial u}{\partial r} \quad (9)$$

and

$$\begin{aligned} \rho u &= \frac{1}{r} \frac{\partial \psi}{\partial r} \\ \rho v &= - \frac{1}{r} \frac{\partial \psi}{\partial x} \end{aligned} \quad (10)$$

Employing Eqs. (1) and (2), all of the governing differential equations, Eqs. (1) through (4), can be converted into the following general form for axisymmetric flow (see Ref. 11 for details)

$$\begin{aligned} a_\phi \left[ \frac{\partial}{\partial x} \left( \phi \frac{\partial \psi}{\partial r} \right) - \frac{\partial}{\partial r} \left( \phi \frac{\partial \psi}{\partial x} \right) \right] - \frac{\partial}{\partial x} \left[ b_{\phi_1} r \frac{\partial C \phi \phi}{\partial x} \right] \\ - \frac{\partial}{\partial r} \left[ b_{\phi_2} r \frac{\partial C \phi \phi}{\partial r} \right] + r d_\phi = 0 \end{aligned} \quad (11)$$

where the coefficients  $a_\phi$ ,  $b_\phi$ ,  $c_\phi$ , and  $d_\phi$  are tabulated in TABLE I for each of the dependent variables under consideration. Use of vorticity and stream function as dependent variables of the governing equations eliminates direct solution of velocity and pressure. However, the primitive variables may be recovered by application of the stream function relations, Eq. (10), and by integration of momentum equations, Eq. (3), respectively. Certain simplifications can be imposed to simplify the energy equation which is very cumbersome because of the complicated ' $d_\phi$ ' term. For example, by assigning the value of unity to the effective Prandtl number and Schmidt numbers the entire ' $d_\phi$ ' term can be eliminated. Justification for this simplification comes from our knowledge of turbulent flows of gases and gas mixtures where the exchange coefficients for heat, mass, and momentum are known to be of very similar magnitude. In addition, the function  $S_\omega$  in the vorticity equation ' $d_\phi$ ' term which is given by

**TABLE I**  
**COEFFICIENTS OF GENERAL ELLIPTIC EQUATION**

$$a_{\phi} \left\{ \frac{\partial}{\partial x} \left( \phi \frac{\partial \psi}{\partial r} \right) - \frac{\partial}{\partial r} \left( \phi \frac{\partial \psi}{\partial x} \right) \right\} - \frac{\partial}{\partial x} \left\{ b_{\phi_1} r \frac{\partial c_{\phi} \phi}{\partial x} \right\} - \frac{\partial}{\partial r} \left\{ b_{\phi_2} r \frac{\partial c_{\phi} \phi}{\partial r} \right\} + r d_{\phi} = 0$$

FUNCTION $\phi$	$a\phi$	$b\phi_1$	$b\phi_2$	$c\phi$	$d\phi$
$m_i$	1.0	$\Gamma_{i \text{ eff}}$	$\Gamma_{i \text{ eff}}$	1.0	$-r_i$
$F$	0	0	$\frac{-1.0}{(K_a + K_s + \frac{1}{r})}$	1.0	$-K_a (F - \sigma T^4) - \frac{K_s}{2} (G - F)$
$G$	0	$\frac{-1.0}{(K_a + K_s)}$	0	1.0	$-\frac{K_a}{r} (G - \sigma T^4) - \frac{K_s}{2r} (G - F)$
$H$	1.0	$\Gamma_h$	$\Gamma_h$	1.0	$-\frac{1}{r} \frac{\partial}{\partial x} \left[ \mu_{\text{eff}} r \left\{ \left( 1 - \frac{1}{Pr} \right) \frac{\partial v^2/2}{\partial x} + \sum_i \left( \frac{1}{Sc} - \frac{1}{Pr} \right) h_i \frac{\partial m_i}{\partial x} \right\} \right] - \frac{1}{r} \frac{\partial}{\partial r} \left[ \mu_{\text{eff}} r \left\{ \left( 1 - \frac{1}{Pr} \right) \frac{\partial v^2/2}{\partial r} + \sum_i \left( \frac{1}{Sc} - \frac{1}{Pr} \right) h_i \frac{\partial m_i}{\partial r} \right\} \right] + Q^R$
$rv_t$	1.0	$\mu_{\text{eff}} r^2$	$\mu_{\text{eff}} r^2$	$\frac{1}{r^2}$	0
$\frac{\omega}{r}$	$r^2$	$r^2$	$r^2$	$\mu_{\text{eff}}$	$-\frac{\partial}{\partial x} (\rho v_t^2) - r \left[ \frac{\partial}{\partial x} \left( \frac{u^2 + v^2}{2} \right) \frac{\partial \rho}{\partial r} - \frac{\partial}{\partial r} \left( \frac{u^2 + v^2}{2} \right) \frac{\partial \rho}{\partial x} \right] - r^2 S_{\omega}$
$\psi$	0	$\frac{1}{\rho r^2}$	$\frac{1}{\rho r^2}$	1.0	$-\frac{\omega}{r}$

$$S\omega = \frac{2}{r} \left[ \nabla (i_r \cdot v) \cdot \nabla (i_x \cdot \nabla \mu_{eff}) + \nabla (i_r \cdot v) \cdot \nabla (i_r \cdot \nabla \mu_{eff}) - \nabla (\nabla \cdot v) \cdot \nabla \mu_{eff} \right] \quad (12)$$

is excluded from the computation, an omission which may be expected to result in only small errors. These terms can be included readily if circumstances are encountered where they might be significant. In the numerical solution procedure, all equations are solved in the form of Eq. (11).

Outside of boundary conditions, to close the system of equations, there remains to specify a turbulence model, a chemistry model, and a radiation model to define effective viscosity, chemical species production, and radiation heat flux, respectively. These models are discussed separately below.

#### II-B.1. Turbulence Model

The flow in furnaces is known to be predominantly turbulent. In order to account for this turbulent behavior in the solution of the governing time-mean equations of motion, a turbulence model is introduced to define the effective viscosity. An historical review and account of turbulence models is available in the literature (see, for instance, Ref. 14). Prandtl (Ref. 15) was perhaps the first to introduce a turbulence model when he postulated that time-averaged shear stresses and time-averaged velocities are proportional as in laminar flow and, furthermore, that the length scale which enters into proportionality, which he called the mixing length, is proportional to the turbulent shear region thickness. Prandtl's mixing length model has been employed successfully by a number of investigators (for example, see Refs. 16 through 20) in a variety of problems primarily involving turbulent motion along walls and in free turbulent flows. A disadvantage of the mixing length model is that it is an equilibrium model (i.e., turbulence is presumed to be produced and dissipated locally) and requires an ad hoc mixing length distribution. Use of more advanced turbulence models requiring solution of additional differential equations would serve to eliminate these limitations; however, the development of these sophisticated models is in the formative stages and successful applications of these techniques to practical flow problems has not been clearly demonstrated.

In view of the early stage of development of the more sophisticated turbulence models, a mixing length model has been employed in the present analysis. The mixing length model was partially developed for use with the FREP code under a jointly sponsored FAA/WPAFB-APL contract, No. F33615-72-C-2042. The formulation of the turbulence model employed in the analysis is based on an evaluation of the mixing length from the work of Williamson (Ref. 19) and Lilley (Ref. 20) with a correction added to the Williamson model to account for the swirling flow. Williamson's model, which is derived from the flow in ducts and channels, is employed in the main body of flow away from the injection ports which are located near the axis of a representative burner (IGT) under consideration. Lilley's model, which includes a correction for swirling flow, is directly applicable to free jet flows and is employed in the vicinity of the injection ports. Transition between the two models is accomplished by monitoring the cross over point of the mixing lengths computed for each model at each axial station taking care to ensure that a smooth transition occurs. If there is no cross over, the Lilley model is used. In mathematical terms the mixing length expression, as employed in this study, for effective viscosity in the  $rx$  and  $r\theta$  directions for the case of axisymmetric swirling flow takes the form (Ref. 21)

$$\begin{aligned} \mu_{rx} = & \mu_{LAM} + \rho l^2 \sqrt{2} \left\{ \left( \frac{\partial u}{\partial x} \right)^2 + \left( \frac{\partial v}{\partial r} \right)^2 + \left( \frac{v}{r} \right)^2 \right. \\ & \left. + \frac{1}{2} \left( \frac{\partial u}{\partial r} \right)^2 + \frac{1}{2} \left[ r \frac{\partial}{\partial r} \left( \frac{\omega}{r} \right) \right]^2 + \frac{1}{2} \left[ \frac{\partial v_t}{\partial x} \right]^2 \right\}^{1/2} \end{aligned} \quad (13)$$

$$\mu_{r\theta} = \frac{\mu_{rx}}{\sigma_{r\theta}} \quad (14)$$

where the mixing length,  $l$ , is given by either Williamson's model

$$\frac{l}{r_0} = 1.75 \lambda e^{(1-y/r)} (y/r_0) \quad (15)$$

or Lilley's model

$$\frac{l}{r_0} = \lambda \left( \frac{r}{r_0} \right) \frac{u}{u_m} = 0.05 \quad (16)$$

where

$$\lambda = 0.08 (1 + \lambda_s S_x) \quad (17)$$

$$\lambda_s = 0.60 \quad (18)$$

$$S_x = G_\theta / (G_x \cdot r \frac{u}{u_m} = 0.01) \quad (19)$$

and

$$\sigma_{r\theta} = 1.0 + 5.0 S_x^{1/3} \quad (20)$$

The factor  $(1+\lambda_s S_x)$  represents the stretching of the length scale due to swirl, the mixing length parameter,  $\lambda$ , approaching an acceptable nonswirling value of 0.08 for the case of no swirl. Constants in Eqs. (15) through (20) have been determined from comparisons of predictions with experimental data. The turbulence model employed in this study represents then an extension of Prandtl's isotropic mixing length model in that nonisotropy of the viscosity is accounted for through definition of the variable  $r\theta$  viscosity, Eq. (14), and through linking of the  $rx$  and  $r\theta$  shear through Eq. (13).

In implementation of the effective viscosity, defined by Eqs. (13) through (20), a difficulty arises in regions close to the wall if grid spacing cannot be refined sufficiently to resolve the large flow gradients occurring there. In the event grid resolution in the near wall region is poor, errors in the local flow properties will occur and be propagated into the main body of flow. To prevent this occurrence, a universal velocity profile known to be accurate in the vicinity of the walls is imposed on the solution at the near wall nodes. This well-known universal velocity distribution, which is referred to as the 'law of the wall', has the form (Ref. 22)

$$u^+ = \frac{1}{C_1} \ln(1 + y^+) + \left[ \left(1 - \frac{1}{C_1} - C_2 a\right) y^+ - C_2 \right] e^{-ay^+} + C_2 \quad (21)$$

where

$$u^+ = \frac{u}{\sqrt{\tau_w / \rho}} \quad (22)$$

$$y^+ = \frac{\rho y \sqrt{\tau_w / \rho}}{\mu} \quad (23)$$

The constants  $a$ ,  $C_1$ , and  $C_2$  are empirically determined. With the proper velocity distribution and, consequently, also the velocity gradient computed at the near wall nodes from Eq. (21), the effective viscosity can then be computed from

$$\mu_{rx} = \mu_{LAM} + \rho \ell^2 \left\{ \left( \frac{\partial u}{\partial r} \right)^2 + \left[ r \frac{\partial}{\partial r} \left( \frac{\omega}{r} \right) \right]^2 \right\}^{1/2} \quad (24)$$

which is the boundary layer equivalent of Eq. (13) which is appropriate for application near the wall. Implicit in the application of Eqs. (21) through (24) is the assumption that normal to the wall the shear stress in the immediate vicinity of the wall is constant. Thus, specifying the velocity and velocity gradient at the near wall nodes in this fashion is equivalent to assigning a 'slip' velocity at the wall itself and imposes an artificial

velocity distribution between the wall and its adjacent nodes. Flow resolution in the narrow region very close to the wall, however, is of little importance in the present task and, hence, the use of the law of the wall is a small price to pay for the high accuracy attainable in the major portion of the flow field. However, in the event accurate heat and mass fluxes at the wall are desirable at a future time, refinements to the wall flux procedure can be easily implemented within the framework of the computational procedure.

### II-B.2. Chemistry Model

Closure of the governing system of equations, Eqs. (1) through (6), requires specification of the rate expression,  $r_i$ , in the chemical species equations, Eq. (2). However, because only nitric oxide chemistry is kinetically treated in this investigation, only an expression for rate of production of nitric oxide need be formulated. To develop the rate of expression for nitric oxide requires knowledge of concentrations of species entering into the nitric oxide reaction scheme which are dependent upon the hydrocarbon fuel (methane,  $\text{CH}_4$ , in this case) combustion process. Under this study, combustion of the hydrocarbon fuel is treated from chemical equilibrium considerations and, as a consequence, concentrations for products of combustion to be employed in the nitric oxide rate expression are computed in a straightforward manner from a chemical equilibrium analysis. Justification for the hydrocarbon equilibrium model is based on the observation that, under pressure and temperature conditions generally existing in burners, fuel oxidation reactions can be expected to go to completion rapidly compared to nitric oxide formation rates. Thus, the chemistry model employed in the analysis consists of two parts: a hydrocarbon oxidation process which is considered to be mixing controlled and a nitric oxide formation process which is kinetically controlled. Also, within the analysis, because the nitric oxide is considered a trace species (i.e., its' concentration is low enough to have little influence on mixture properties), the nitric oxide and hydrocarbon chemistry is uncoupled in the solution procedure. Hence, the nitric oxide species equation is solved separately from the other equations and only at the end of the iteration process after final converged values for all flow variables have been determined. The two components of the chemistry model, representing the equilibrium hydrocarbon chemistry analysis and the finite-rate nitric oxide analysis, are discussed separately in detail below.



## II-B.2i. Nitric Oxide Chemical Analysis

Solution of the species equations to account for convection, diffusion, and production of nitric oxide requires definition of an expression describing rate of creation of nitric oxide (see Eq. (2)). In order to develop this expression, knowledge of the reaction mechanism by which nitric oxide is formed is required. A generally accepted reaction scheme for nitric oxide formation and decomposition in post flame gases is that proposed by Lavoie, et al., (Ref. 23). It consists of the following six reactions:



The first two reactions, Eqs. (25) and (26), form the Zeldovitch mechanism (Ref. 24) and is considered to be the principal nitric oxide formation reaction mechanism. These two reactions together with the third reaction, Eq. (27), which assumes minor importance under fuel rich conditions, form the extended Zeldovitch mechanism which is employed in the present study. At low temperatures when nitric oxide concentrations are much greater than equilibrium values, the fourth, fifth, and sixth reactions, Eqs. (28) through (30), involving  $\text{N}_2\text{O}$  as intermediary, may become important; however, because overall reaction rates are so low, the net effect of these reactions is probably negligible and, therefore, these reactions have been neglected in the present analysis. The results of Bowman and Seery (Ref. 25), in investigation of nitric oxide formation kinetics in combustion pressures, lend support to this approach and it has been followed by other investigators (Refs. 5 and 27).

With the reaction mechanisms for nitric oxide formation defined by the extended Zeldovitch mechanism, Eqs. (25) through (27), it becomes possible to develop an expression for the rate term,  $r_1$ , entering in the chemical species equation, Eq. (2). The mathematical development of the rate term has as its basis the 'Law of Mass Action' which states that the rate of chemical reaction is proportional to the active masses of the reacting materials. Thus, referring to Eqs. (25) through (27), rate expressions for nitric oxide and nitrogen can be written

$$\begin{aligned} \frac{d[\text{NO}]}{dt} = & k_{1b} [\text{N}_2] [\text{O}] + k_{2f} [\text{N}] [\text{O}_2] + k_{3f} [\text{N}] [\text{OH}] \\ & - k_{1f} [\text{N}] [\text{NO}] - k_{2b} [\text{NO}] [\text{O}] - k_{3b} [\text{NO}] [\text{H}] \end{aligned} \quad (31)$$

$$\begin{aligned} \frac{d[\text{N}]}{dt} = & k_{1b} [\text{N}_2] [\text{O}] + k_{2b} [\text{NO}] [\text{O}] + k_{3b} [\text{NO}] [\text{H}] \\ & - k_{1f} [\text{N}] [\text{NO}] - k_{2f} [\text{N}] [\text{O}_2] - k_{3f} [\text{N}] [\text{OH}] \end{aligned} \quad (32)$$

where  $[ ]$  denotes moles per unit volume and  $k_b$  and  $k_f$  are the rate constants (volume/mole-sec) in the backward and forward directions, respectively. Because relaxation times for Eq. (32) are several orders of magnitude shorter than for Eq. (31), it is a good approximation to assume steady concentration for  $[\text{N}]$ . Therefore, setting  $d\text{N}/dt = 0$ , Eq. (32) can be solved for  $[\text{N}]$  as

$$[\text{N}] = \frac{k_{1b} [\text{N}_2] [\text{O}] + k_{2b} [\text{NO}] [\text{O}] + k_{3b} [\text{NO}] [\text{H}]}{k_{1f} [\text{NO}] + k_{2f} [\text{O}_2] + k_{3f} [\text{OH}]} \quad (33)$$

Equation (31) can now be written

$$\begin{aligned} \frac{d[\text{NO}]}{dt} = & k_{1b} [\text{N}_2] [\text{O}] - k_{2b} [\text{NO}] [\text{O}] - k_{3b} [\text{NO}] [\text{H}] \\ & + [\text{N}] \{ k_{2f} [\text{O}_2] + k_{3f} [\text{OH}] - k_{1f} [\text{NO}] \} \end{aligned} \quad (34)$$

where  $[N]$  is obtained from Eq. (33). Equation (34) is the desired rate expression for  $[NO]$  in terms of concentrations of  $N_2$ ,  $O$ ,  $H$ ,  $O_2$ , and  $OH$  which are obtained from an equilibrium hydrocarbon air combustion analysis, discussed in detail below. The dimensionally correct expression for the rate term,  $r_1$ , to be employed in solution of Eq. (2) is

$$r_1 = M_{NO} \frac{d[NO]}{dt} \quad (35)$$

The rate constants governing the nitric oxide reaction scheme, Eqs. (25) through (27), and utilized in the rate expression, Eq. (34), are employed in the solution procedure in modified Arrhenius form, i.e.,

$$k_j = A_j T^{N_j} \exp(-B_j/RT) \quad (36)$$

where data for the activation energies,  $B_j$ , the frequency factors,  $A_j$ , and exponent,  $N_j$ , are taken from Refs. 27 and 28 and tabulated in TABLE II.

#### II-B.2ii. Equilibrium Hydrocarbon Air Combustion Analysis

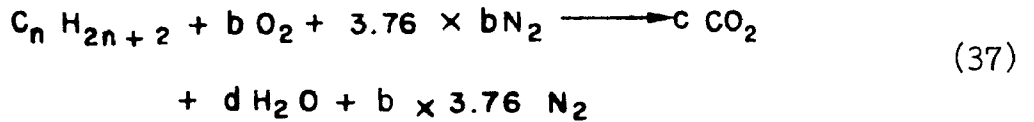
In order to determine the state of the burnt gases and provide the necessary information concerning concentrations of species entering into the nitric oxide rate expression, Eq. (35), an equilibrium hydrocarbon-air combustion model is employed in this investigation. Chemical equilibrium is that condition under which the forward and reverse speeds of a chemical reaction are equal and, hence, concentrations of reactants and products may be determined. In the present analysis, the equilibrium hydrocarbon model is implemented by first determining fuel-air ratios by solution of the governing species diffusion equations without rate terms (i.e., assuming the combustion process to be mixing controlled), followed by implementation of an equilibrium hydrocarbon-air computational routine to establish coexisting concentrations of products of combustion at the existing temperature and pressure conditions. The equilibrium computational analysis employed for the hydrocarbon-air combustion model is based on the work of Brinkley (Refs. 29 and 30). For a brief account of the approach, consider a chemically correct reaction of a representative paraffinic hydrocarbon with air

**TABLE II**  
**CHEMICAL RATE CONSTANTS**

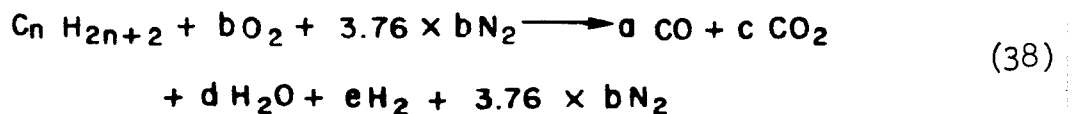
$$k = A T^N \exp (-B/RT)^*$$

REACTION	FORWARD RATE			REVERSE RATE		
	A	B	N	A	B	N
$\text{NO} + \text{N} \rightleftharpoons \text{O} + \text{N}_2$	$3.10 \times 10^{13}$	334.	0	$1.36 \times 10^{14}$	75400.	0
$\text{N} + \text{O}_2 \rightleftharpoons \text{NO} + \text{O}$	$6.43 \times 10^9$	6250.	1.0	$1.55 \times 10^9$	38640.	1.0
$\text{N} + \text{OH} \rightleftharpoons \text{NO} + \text{H}$	$4.22 \times 10^{13}$	0	0	$1.64 \times 10^{14}$	48600.	0

\* UNITS ARE CM, CAL, °K, g-MOLE, SEC AND ATM



To solve Eq. (37) for the concentration of the products of reaction, the coefficients b, c, and d must be determined. For this purpose the required number of additional equations for an atom balance can be written between C, O, or H atoms resulting in an algebraic set of three equations which can be solved for the three unknowns. The high temperature levels commonly encountered in combustion devices justify the assumption that the hydrocarbon-air reaction goes to completion as implied by Eq. (37); however, in the usual case, the mixture of hydrocarbon fuel and air is not stoichiometric as indicated. For the general case of fuel rich or fuel lean mixture the products of combustion, in addition to CO<sub>2</sub>, H<sub>2</sub>O, and N<sub>2</sub>, may also include CO, H<sub>2</sub>, O<sub>2</sub>, OH, H, and O atoms and radicals and other less populous constituents. To solve for the concentration of these additional species, it is recognized that additional equations are required to define additional unknown coefficients. Therefore, auxiliary reactions for which equilibrium constants are known are employed to provide the required additional equations. These additional equations are written in terms of the unknown species concentrations and the known equilibrium constants. As a simple illustration, consider the case of two additional unknowns, as for example, in the following reaction



In addition to the reaction equation three equations can be written on the basis of a C, O, and H atom balance; however, there are five unknowns, a, b, c, d, and e. The necessary fifth equation is obtained from an auxiliary reaction for which the equilibrium constant is known. For example, the water-gas reaction can be written



from which the known equilibrium constant,  $k_p$ , would be written as

$$k_p = \frac{a d}{c e} \quad (40)$$

resulting in five equations from which the five unknowns coefficients can be determined. The choice of additional reactions is somewhat arbitrary and can vary depending on local fuel-air rates and temperature conditions, in order to optimize the iterative solution procedure. In the present case, a test is made of the oxygen concentration and depending on its magnitude relative to the carbon and hydrogen concentration, three possible sets of additional reactions are employed. These three cases are listed in TABLE III. Depending on which of the three categories the oxygen concentration falls into, the presumed primary products of combustion are indicated along with five representative auxiliary equations which may be employed in the reaction scheme for which equilibrium constants are known. The equilibrium constants for the auxiliary equations are obtained from the data tabulated in reference 31. Thus, with the equations obtained from the atom balance and additional equations provided by the auxiliary equilibrium reactions, the problem is completely specified and the unknown concentrations (some of which are employed in the nitric oxide expression, Eq. (34)), are solved for using a Newton-Raphson numerical iterative procedure.

### II-B.3 Radiation Model

The purpose of the radiation model employed under this investigation is to define the radiant energy contribution to combustion heat transfer rates. It is employed specifically in the analysis to define the radiant heat flux term,  $Q_R$ , entering in the energy equation, Eq.(4), through which coupling between radiation, convection, and conduction modes of heat transfer occurs. The radiative heat transfer process is inherently different from conductive and convective heat transfer processes in that, in the two latter cases, the energy is transferred by molecular collision and transport whereas, in the radiative process, energy transfer is in the form of electromagnetic waves, not requiring contact of the molecules. Radiation becomes of importance

**TABLE III**  
**AUXILIARY REACTIONS FOR HYDROCARBON COMBUSTION EQUILIBRIUM MODEL**

	CASE I	CASE II	CASE III
OXYGEN CONCENTRATION	$\{ [C] + [H]/2 \} \geq [O] \geq [C]$	$\{ 2[C] + [H]/2 \} \geq [O] \geq \{ [C] + [H]/2 \}$	$[O] \geq \{ 2[C] + [H]/2 \}$
PRINCIPAL PRODUCTS	$H_2, H_2O, CO$	$H_2O, CO, CO_2$	$H_2O, CO_2, O_2$
AUXILIARY REACTIONS	$CO + H_2O \rightleftharpoons CO_2 + H_2$ $2H_2O \rightleftharpoons O_2 + 2H_2$ $H_2O \rightleftharpoons O + H_2$ $1/2 H_2 \rightleftharpoons H$ $H_2O \rightleftharpoons OH + 1/2 H_2$	$CO + H_2O \rightleftharpoons CO_2 + H_2$ $2CO_2 \rightleftharpoons 2CO + O_2$ $1/2 CO + 1/2 H_2O \rightleftharpoons 1/2 CO_2 + H$ $1/2 CO_2 + 1/2 H_2O \rightleftharpoons 1/2 CO + OH$ $CO_2 \rightleftharpoons CO + O$	$H_2O \rightleftharpoons H_2 + 1/2 O_2$ $1/2 H_2O \rightleftharpoons H + 1/4 O_2$ $H_2O + 1/2 O_2 \rightleftharpoons 2OH$ $1/2 O_2 \rightleftharpoons O$ $CO_2 \rightleftharpoons CO + 1/2 O_2$



relative to conduction and convection when there is appreciable conversion between electromagnetic and molecular kinetic energy within the system, which may occur, for example, if the medium is absorbing and emitting, as is generally the case in combustion chambers.

The radiant heat transfer model employed under this analysis takes the form of a discrete-flux model. This model has been employed successfully by a number of investigators (Refs. 32 through 39) and is described in the literature (Refs. 35 and 36). A basic hypothesis of discrete flux models is that the net radiant flux passing through a unit area in each coordinate direction, is presumed to consist of contributions from collimated forward and backward fluxes. Thus, in the present two-dimensional axisymmetric flow case, four fluxes are considered. The configuration of interest is illustrated in Fig. 1 in terms of one coordinate direction only, representing the two fluxes, K and L, in the forward and backward axial directions, respectively. If the monochromatic intensity of radiant energy traveling in the direction  $\Omega$  is represented by  $K_\lambda$ , then the total flux of radiant energy passing forward through the unit plane which is perpendicular to the x-axis is given by the integral

$$K = \int_{\lambda=0}^{\lambda=\infty} 2\pi \int_{\theta=0}^{\theta=\pi/2} K_\lambda \cos \theta \sin \theta d\theta d\lambda \quad (41)$$

Similarly, the total flux passing backward in the negative x-direction through the unit area is

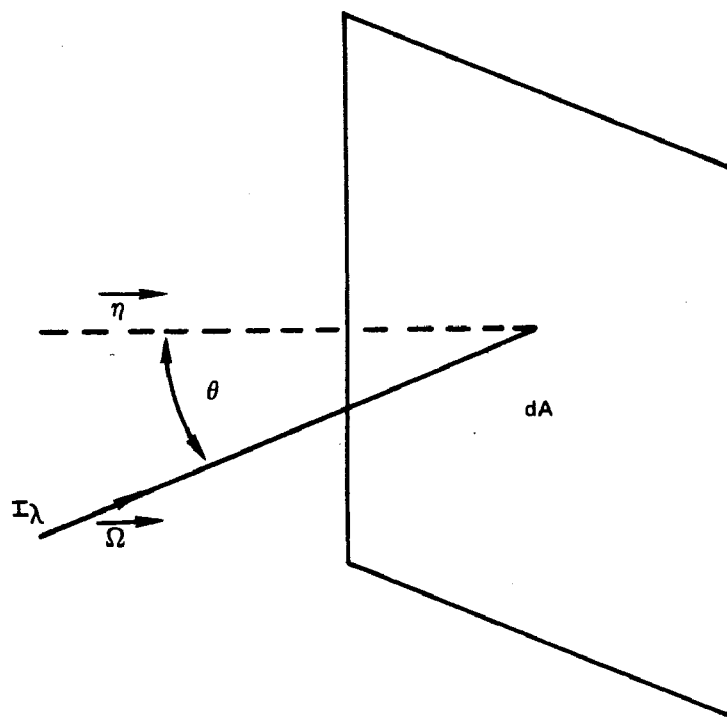
$$L = \int_{\lambda=0}^{\infty} 2\pi \int_{\theta=\pi}^{\theta=\frac{3\pi}{2}} L_\lambda \cos \theta \sin \theta d\theta d\lambda \quad (42)$$

and the net flux passing through the area is

$$\text{NET AXIAL RADIATION FLUX} = K - L \quad (43)$$

which has units of energy per unit area per unit time. Similar relationships can be deduced for I and J fluxes passing forward and backward in the radial direction, respectively. Thus, the net flux in the radial direction is written

## COORDINATE SYSTEM FOR RADIANT FLUX



$$\text{NET RADIAL RADIATION FLUX} = I - J \quad (44)$$

Employing Eq. (43) and Eq. (44), the radiant heat flux term,  $Q_R$ , appearing in the energy equation, Eq. (4), and requiring definition, can be written for the axisymmetric flow case as

$$Q_R = \left\{ \frac{1}{r} \frac{\partial}{\partial r} \left[ r(I-J) \right] + \frac{\partial}{\partial x} (K-L) \right\} \quad (45)$$

In order to derive relationships for the I, J, K, and L fluxes required to define  $Q_R$ , reference is made to energy losses and gains incurred by a collimated flux of radiation as it travels an incremental distance. Energy losses are incurred by absorption and scattering and energy gains incur by scattering from the backward flux and by thermal emission from the incremental element. For an isotropic, gray (absorption coefficient independent wave-length) medium this transport process can be described by the following equations for each of the two axisymmetric coordinate directions:

$$\frac{d}{dr} (rI) = r \left\{ -(K_a + K_s) I + \frac{J}{r} + K_a \sigma T^4 + \frac{K_s}{4} (I+J+K+L) \right\} \quad (46)$$

$$\frac{d}{dr} (rJ) = r \left\{ (K_a + K_s) J + \frac{J}{r} - K_a \sigma T^4 - \frac{K_s}{4} (I+J+K+L) \right\} \quad (47)$$

$$\frac{dK}{dx} = -(K_a + K_s) K + K_a \sigma T^4 + \frac{K_s}{4} (I+J+K+L) \quad (48)$$

$$\frac{dL}{dx} = (K_a + K_s) L - K_a \sigma T^4 - \frac{K_s}{4} (I + J + K + L) \quad (49)$$

where  $\sigma$  is the Stefan-Boltzmann constant,  $T$  is absolute temperature,  $K_a$  is an absorption coefficient, and  $K_s$  is a scattering coefficient. With the equations written in this form, it is seen that one-quarter of the total scattered radiation is presumed to go into each of the four backward and forward directions. Also, it is to be noted that the equations are consistent with the solution  $I = J = K = L = \sigma T^4$  so that in an equilibrium situation,  $\sigma T^4$  represents the flux across any plane.

Before solution to the set of four radiation transport equations, Eqs. (46) through (49), can be attempted, information regarding the mean absorption coefficients,  $K_a$ , and scattering coefficients,  $K_s$ , is required. However, because scattering can be considered to be of secondary importance in the particle-free gaseous medium under study here, definition of scattering coefficients becomes unnecessary and, hence, omitted in the analysis. For an evaluation of the absorption coefficients, reliance is placed on the considerable amount of data available on emissivity of gases and mixture of gases (Refs. 37 and 38) from which values for absorption coefficients can be extracted. For example, conversion between emissivity data and absorption coefficients can be shown (Ref. 35) to be governed by the following relationship

$$K_a = \frac{1}{2} \left( \frac{\epsilon}{L_0} \right)_{L_0 \rightarrow 0} \quad (50)$$

where  $L_0$  is a characteristic gas-thickness, in this case, taken to be a representative grid spacing. The indicated extrapolation in Eq. (50) is due to the fact that the concept of gas emissivity refers to an isothermal gas and a radiating gas approaches isothermal conditions only in the limit. Employing Eq. (50), absorption coefficients for air, water vapor, and carbon dioxide are reported by Cess (Ref. 35).

Once the absorption coefficients are determined to implement the radiation model, it remains to solve the radiation transport equations, Eqs. (46) through (49), in the computational procedure. As an alternative, however, a considerable simplification can be realized by recasting these equations in alternate form, whereby it will only be necessary to solve two

additional equations instead of the four. For this purpose the following definitions are made (the scattering coefficient,  $K_s$ , is retained in the subsequent mathematical development, for generality):

$$F = (I + J)/2 \quad (51)$$

$$Q = I - J \quad (52)$$

$$G = (K + L)/2 \quad (53)$$

$$R = K - L \quad (54)$$

The manipulation of Eqs. (46) and (47) with Eqs. (51) and (52) leads to

$$Q = \frac{-2}{\left(K_a + K_s + \frac{1}{r}\right)} \frac{dF}{dr} \quad (55)$$

and

$$\frac{d(rQ)}{dr} = 2K_a r (\sigma T^4 - F) + K_s r (G - F) \quad (56)$$

and the combination of Eqs. (55) and (56) can be written

$$\frac{d}{dr} \left[ \frac{r}{K_a + K_s + \frac{1}{r}} \frac{dF}{dr} \right] = K_a r (F - \sigma T^4) + \frac{K_s r}{2} (F - G) \quad (57)$$

Similarly, Eqs. (48) and (49), together with Eqs. (53) and (54), can be manipulated to yield

$$R = \frac{-2}{K_a + K_s} \frac{dG}{dx} \quad (58)$$

$$\frac{dR}{dx} = 2 K_a (\sigma T^4 - G) + K_s (F - G) \quad (59)$$

and the combination of Eqs. (58) and (59) is written

$$\frac{d}{dx} \left( \frac{1}{K_a + K_s} \frac{dG}{dx} \right) = K_a (G - \sigma T^4) + \frac{K_s}{2} (G - F) \quad (60)$$

Equations (57) and (60) represent the two differential equations of interest. Solution of these two equations indirectly provides all the information required to define the heat flux term,  $Q_R$ , in the energy equation. For example, with distribution of  $F$  and  $G$  provided by solution of Eqs. (57) and (60) in the iterative solution procedure,  $Q$  and  $R$  can be determined from Eqs. (55) and (58), respectively. Then, to compute the desired  $I$ ,  $J$ ,  $K$ , and  $L$  fluxes necessary for definition of the radiant heat flux term,  $Q_R$ , in Eq. (45), Eqs. (51) and (52), and Eqs. (53) and (54) can be rearranged so that the following explicit expressions for the derived fluxes, in terms of known values of  $F$ ,  $Q$ ,  $G$ , and  $R$ , may be obtained:

$$I = F + \frac{1}{2}Q \quad (57)$$

$$J = F - \frac{1}{2}Q \quad (58)$$

$$K = G + \frac{1}{2}R \quad (59)$$

$$L = G - \frac{1}{2}R \quad (60)$$

Equations (57) through (60) thus provide the necessary input information to Eq. (45) in terms of forward and backward fluxes in each coordinate direction, to enable definition of the radiant flux term in the energy equation.

## II-C. BOUNDARY CONDITION

Solution of the governing partial differential equations in the form of Eq. (11) is contingent upon specification of boundary conditions for each of the dependent variables under consideration. Equation (11) represents a system of eight partial differential equations for the eight unknowns: vorticity, stream function, stagnation enthalpy, fuel mass fraction, nitric oxide mass fraction, swirl velocity, and the two radiation components representing radiation fluxes in the axial and radial directions (temperature, pressure, density, viscosity, air mass fraction, specific heat, and other mixture properties are deduced from the eight dependent variables by means of auxiliary relationships, as mentioned previously). Because of the elliptic form of the governing conservation equations, boundary conditions for each of the eight variables are required on all the boundaries of the solution domain. These boundaries are indicated by dashed lines in Fig. 2 where a schematic of the furnace under study is illustrated. The boundary conditions for each of the eight dependent variables are given below in terms of normal and tangential coordinates (n,s) to each of the boundary surfaces. With exception of the right (downstream) boundary and the centerline, which are treated separately, other boundary conditions are grouped according to whether the boundary surface is a solid wall or an injection port. (Note: The boundary conditions for the F and G radiation functions require special attention and are given detailed consideration at the end of this section.)

Injection Ports:

$$\xi = -1/r \left( \frac{\partial v_n}{\partial s} - \frac{\partial v_s}{\partial n} \right)$$

$$\psi = \int \rho v_n ds$$

$$H = \sum h_i m_i + KE$$

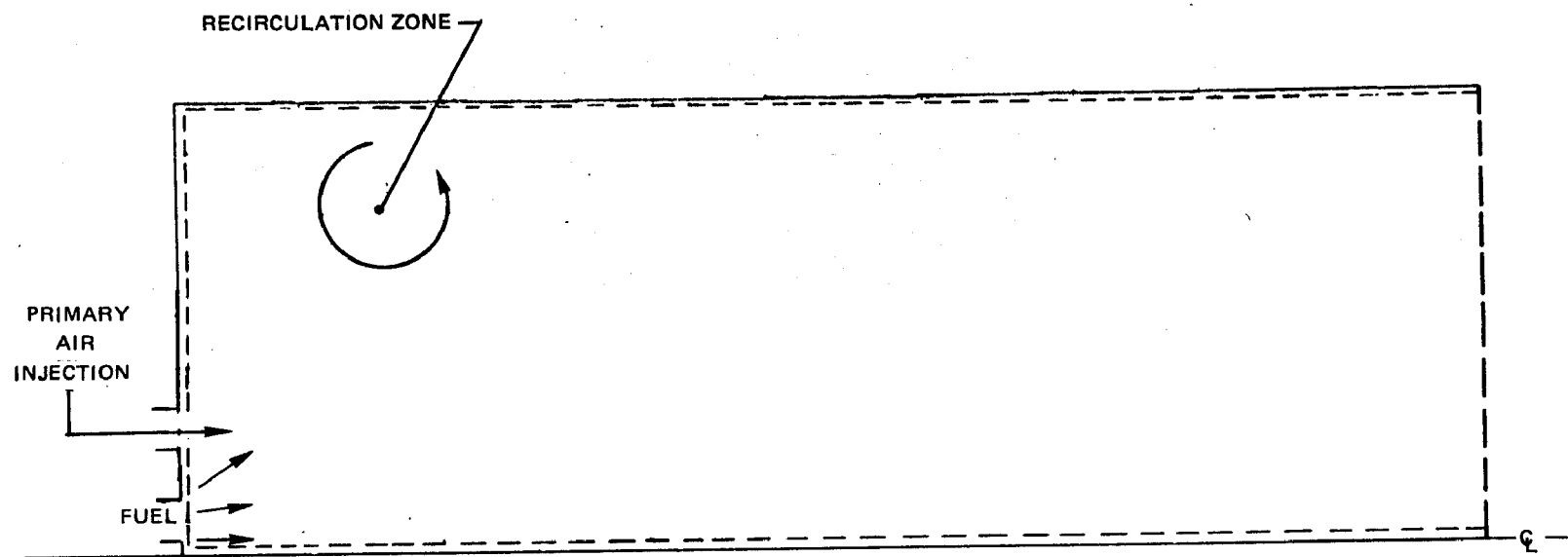
$$m_f = 1 \text{ at fuel port (otherwise zero)}$$

$$m_{NO} = 0$$

$$v_t = c_t u_a \text{ at air port (otherwise zero)}$$



## BURNER FLOW MODEL



Solid Walls:

$$\xi = \frac{1}{r} \frac{\partial v_s}{\partial n}$$

$$\psi = \text{CONST}$$

$$\frac{\partial H}{\partial n} = 0$$

$$\frac{\partial m_f}{\partial n} = 0$$

$$\frac{\partial m_{NO}}{\partial n} = 0$$

$$v_t = 0$$

Centerline:

$$\frac{\partial \xi}{\partial n} = 0$$

$$\psi = \text{CONST}$$

$$\frac{\partial H}{\partial n} = 0$$

$$\frac{\partial m_f}{\partial n} = 0$$

$$v_t = 0$$

Right Boundary:

$$\frac{\partial^2 \xi}{\partial n^2} = 0$$

$$\frac{\partial^2 \psi}{\partial n^2} = 0$$

$$\frac{\partial^2 H}{\partial n^2} = 0$$

$$\frac{\partial^2 m_f}{\partial n^2} = 0$$

$$\frac{\partial^2 m_{NO}}{\partial n^2} = 0$$

$$\frac{\partial^2 r v_t}{\partial n^2} = 0$$

The boundary conditions expressed above are formulated to simulate as near as possible the condition existing in the furnace. At an air port a tangential velocity component is imparted to the inlet flow of " $C_t$ " times the axial velocity. The quantity " $C_t$ " varies according to the degree of swirl required to simulate the actual furnace operating conditions. The velocities at the inlet ports are presumed to be known. Along the solid walls, the boundary conditions reflect the velocity no-slip conditions, the impermeability to mass transfer, and the local heat balance of the walls. In the exit plane, the boundary conditions are formulated to present as little constraint as possible to the flow and the boundary conditions along the centerline are deduced from symmetry conditions.

The radiation boundary conditions in terms of the functions F and G remain to be defined and are derived below. Only the boundary conditions for function F need be formulated as the boundary conditions for the function G can be deduced by analogy. Thus, considering the radial coordinate direction only, the boundary conditions in terms of the radial outward flux I and inward flux J can be written in general form as

$$b_0 + b_1 I + b_2 J = 0 \quad (61)$$

where  $b_0$ ,  $b_1$ , and  $b_2$  are coefficients to be evaluated from known conditions at the boundary. These conditions fall into one of the following three categories.

(1) OPAQUE WALL OF PRESCRIBED TEMPERATURE - In this case the radiation flux at the surface is due to reflection and emission only (transmissivity = 0) and the boundary condition follows as

$$J = (1 - \epsilon_w) I + \epsilon_w \sigma T^4 \quad (62)$$

from which  $b_0$ ,  $b_1$ , and  $b_2$  can be easily deduced to be

$$\begin{aligned} b_0 &= \epsilon_w \sigma T_w^4 \\ b_1 &= (1 - \epsilon_w) \\ b_2 &= -1 \end{aligned} \quad (63)$$

The emissivity of the wall  $\epsilon_w$  is known from experiment or obtained from the literature as a function of wall temperature and composition.

(2) OUTGOING RADIATION ESCAPES - In this case there is no emission or reflection and the radiation flux is just equal to the incoming radiation,  $J_{in}$ . Hence,

$$I = J_{in} \quad (64)$$

and it follows that

$$\begin{aligned} b_0 &= -J_{in} \\ b_1 &= 0 \\ b_2 &= 1 \end{aligned} \quad (65)$$

(3) SYMMETRY AXIS - At a symmetry axis inward and outward fluxes are equal, consequently,

$$I = J \quad (66)$$

and, therefore,

$$\begin{aligned} b_0 &= 0 \\ b_1 &= 1 \\ b_2 &= -1 \end{aligned} \tag{67}$$

The boundary conditions, as developed above, are expressed in terms of I and J fluxes, however, boundary conditions in terms of F are required. In order to convert from boundary conditions in terms of I and J to those for F, Eqs. (51), (52), and (61) are manipulated to give

$$b_0 + (b_1 + b_2) F + \left( \frac{b_1 - b_2}{2} \right) Q = 0 \tag{68}$$

Employing Eq. (55) for Q, Eq. (68) becomes

$$b_0 + (b_1 + b_2) F + \frac{b_2 - b_1}{(K_0 + K_s + \frac{1}{r})} \frac{dF}{dr} = 0 \tag{69}$$

The analogous expression for G in the axial direction is

$$b_0 + (b_1 + b_2) G + \frac{b_2 - b_1}{K_0 + K_s} \frac{dG}{dx} = 0 \tag{70}$$

Substitution of the appropriate values of  $b_0$ ,  $b_1$ , and  $b_2$  in Eqs. (69) and (70) is sufficient to define the boundary condition for the functions F and G on the radial and axial boundary surfaces, respectively.

## SECTION III

### COMPUTATIONAL ANALYSIS

Exact analytical solutions to the time-averaged Navier-Stokes equations are rare due to their high order and coupled nonlinearity. As a result, routine solutions to these equations, to a large extent, can only be obtained by numerical methods. Numerical techniques have undergone significant advances over the years and computational methods for obtaining numerical solution to the Navier-Stokes equations are now available (Refs. 39 through 44). These numerical methods, however, have not proven to be entirely satisfactory for routine use. Early attempts at solving the Navier-Stokes equations (Refs. 39 through 42), for example, suffered mostly from inability to maintain computational efficiency and stability over a sufficiently wide range of flow conditions. In a recent attempt to develop a practical method of routinely solving the Navier-Stokes equations the method of Gosman, et al., (Ref. 43) employed a point relaxation method. However, a point relaxation method is relatively inefficient and, in addition, because of the use of one-sided differencing, the method may be expected to yield less accurate solutions than second-order central difference schemes for the same number of grid points. The recently developed pseudo-time-dependent computational procedure reported by McDonald, et al., (Ref. 44) solves the vorticity and stream function equations separately in the inlet region of a duct. The necessity for evaluating and applying several weighting factors to promote convergence within the procedure leaves some doubt as to the applicability of the method to general problem solving. Furthermore, the McDonald procedure, which applies the alternating-direction-implicit (ADI) algorithm of Peaceman and Rachford (Ref. 45) to the solution of the vorticity-stream function equations, employs values of the ADI iteration parameters which are not permitted to vary in the iteration cycle; a factor which may be expected to detract from the overall efficiency of the method. To overcome shortcomings of previous methods, a novel numerical procedure for solving the time-averaged Navier-Stokes equations has been developed under UARL Corporate-sponsorship. In the present investigation the UARL computational procedure has been further developed to solve the equations governing the flow in a furnace and details of this procedure are presented below.

#### III-A. THE COMPUTATIONAL PROCEDURE

Direct numerical solution of finite-difference approximations to the time-averaged Navier-Stokes equations in the present study is accomplished by implementation of a relaxation procedure. In applying relaxation procedures,

residuals computed at each point of the flow field are reduced (relaxed) to a sufficiently small value by successively updating the approximation to the solution current at that stage within the iterative solution cycle. (Residuals can be defined as deviations of the current solution from the true solution of the difference equations at a particular stage of the iteration cycle.) By analogy with time-dependent methods relaxation procedures may be classified as either implicit or explicit methods, depending on how the differencing is done. Explicit methods are computationally simpler than implicit methods because solution at existing iteration levels can be obtained from known information at previous iteration levels. With implicit methods the information necessary to advance the solution is contained implicitly in the equations and cannot entirely be obtained from known information at the previous iteration level. Consequently, solution by an implicit scheme is obtained by the computationally more troublesome simultaneous solution of the set of finite-difference equations usually either by matrix inversion or Gaussian elimination. Although computationally more troublesome, implicit relaxation schemes can be considerably more efficient (as shown below) than explicit procedures, particularly when practical constraints dictate a large number of grid nodes.

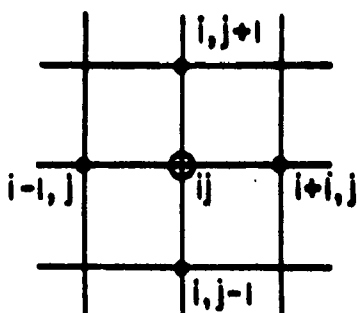
Relaxation procedures are frequently grouped as either point, line, or field methods depending on where in the field residuals are relaxed implicitly. A comparison of the three methods is indicated graphically in Fig. 3 where a representative five-point molecule employed in the present analysis is depicted. As can be seen, a solution is obtained at an individual grid node, along a line of grid nodes or at all nodes throughout the field for the point, line, and field methods, respectively. Hence, it can be concluded from the previous discussion that in advancing from the point to the field methods the computational procedure, although becoming computationally more troublesome, can be expected to become progressively more efficient.

Recognizing the importance of an efficient computational procedure for application to furnace problems, wherein large density of grid points might be required and a large number of governing flow equations might be present, the computational procedure developed at UARL for solving the time-averaged Navier-Stokes equations and employed in the present study is a second-order implicit field relaxation procedure. It employs a novel scheme for derivation of the finite-difference equations which are solved by the Peaceman-Rachford (Ref. 44) alternating-direction-implicit (ADI) algorithm. As evidence of the efficiency of the field (implicit) relaxation procedure in comparison with point (explicit) relaxation procedures, sample computations of the flow in a simple axisymmetric chamber are presented in Fig. 4. For an 11 x 21 grid mesh approximately a threefold improvement in computer efficiency is indicated by the UARL field relaxation procedure in comparison with the point

## RELAXATION PROCEDURES

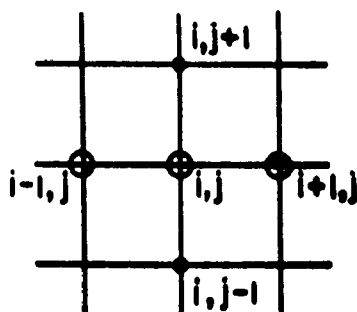
**DEFINITIONS:**

- $\phi$  REPRESENTATIVE VARIABLE
- $R$  RESIDUAL
- $n$  ITERATION INDEX



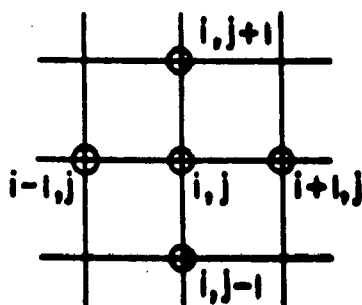
**POINT METHOD  
(EXPLICIT)**

$$a_1 \phi_{ij}^{n+1} = R_{ij}^n + (\text{OTHER } N\text{-LEVEL TERMS})$$



**LINE METHOD  
(IMPLICIT AT GRID POINTS ALONG A LINE)**

$$a_1 \phi_{i+1,j}^{n+1} + a_2 \phi_{ij}^{n+1} + a_3 \phi_{i-1,j}^{n+1} = R_{ij}^n + (\text{OTHER } N\text{-LEVEL TERMS})$$



**FIELD METHOD  
(IMPLICIT AT GRID POINTS OVER ENTIRE FIELD)**

$$a_1 \phi_{i+1,j}^{n+1} + a_2 \phi_{ij}^{n+1} + a_3 \phi_{i-1,j}^{n+1} + a_4 \phi_{i,j+1}^{n+1} + a_5 \phi_{i,j-1}^{n+1} = R_{ij}^n + (\text{OTHER } N\text{-LEVEL TERMS})$$

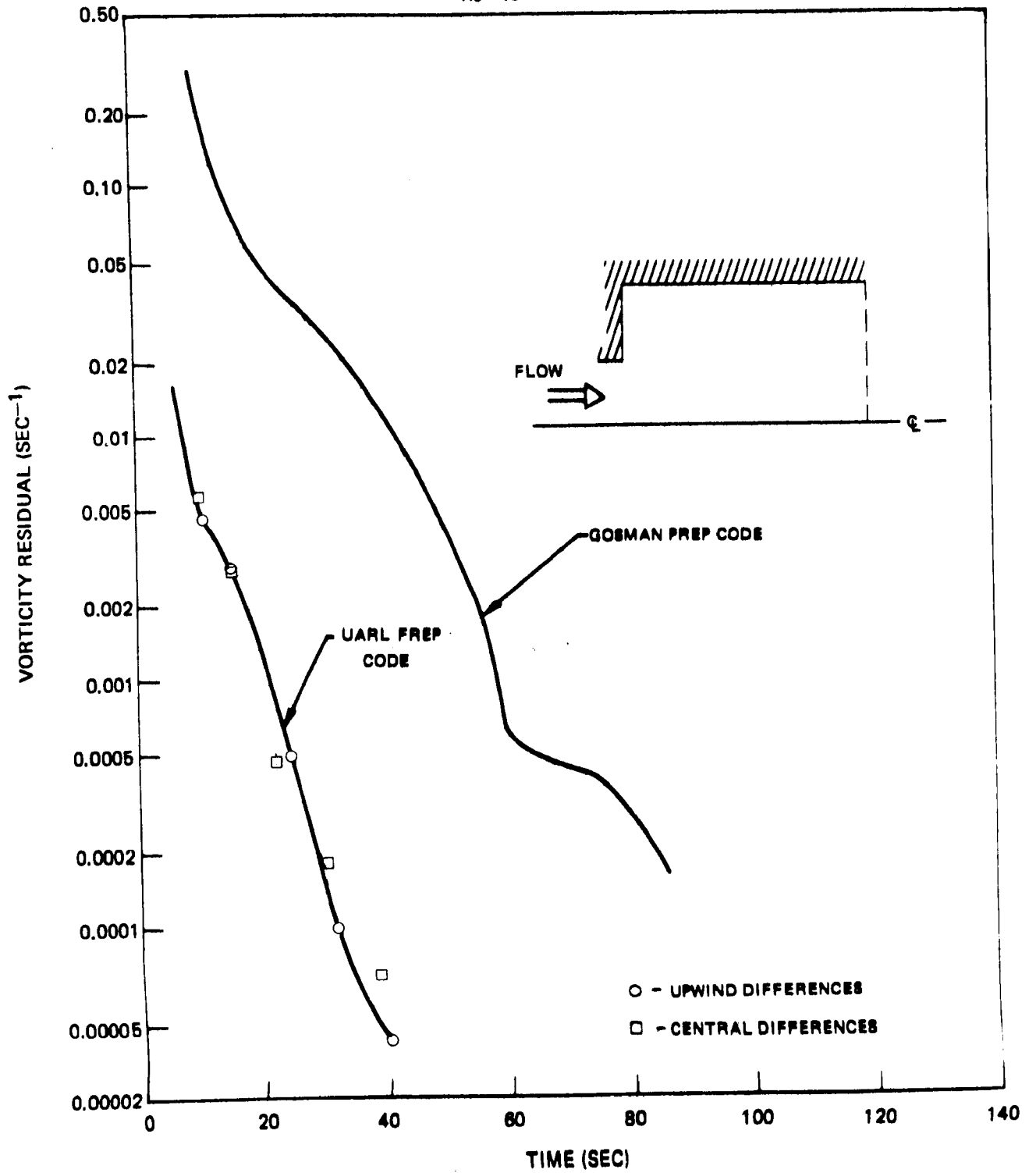


# VORTICITY RESIDUAL HISTORY

AXISYMMETRIC CHAMBER

11x21 GRID

$Re = 10$



relaxation procedure of Gosman, et al. In Fig. 5 the results of the same case are presented for a 31 x 41 grid mesh with resultant improvements in efficiency by the field methods of one order of magnitude or more. Representative velocity profiles for these sample cases are presented in Fig. 6 at two axial locations establishing the identity of the two velocity predictions.

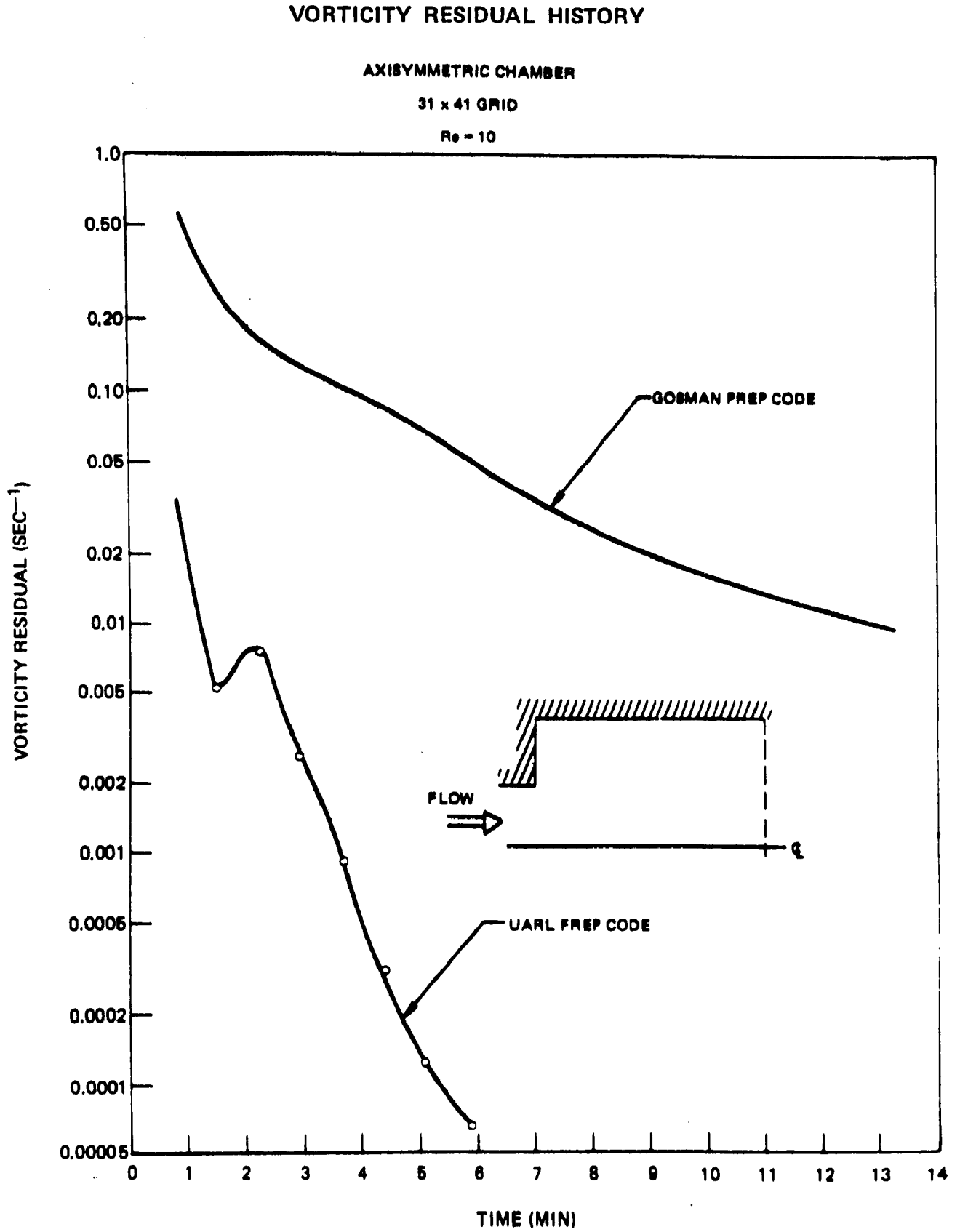
A detailed description of the computational procedure employed in this evaluation, particularly in regard to development of finite-difference equations and the alternating-direction-implicit (ADI) solution procedure employed to solve the difference equation, is presented in the subsequent sections.

### III-B. DEVELOPMENT OF FINITE-DIFFERENCE EQUATIONS

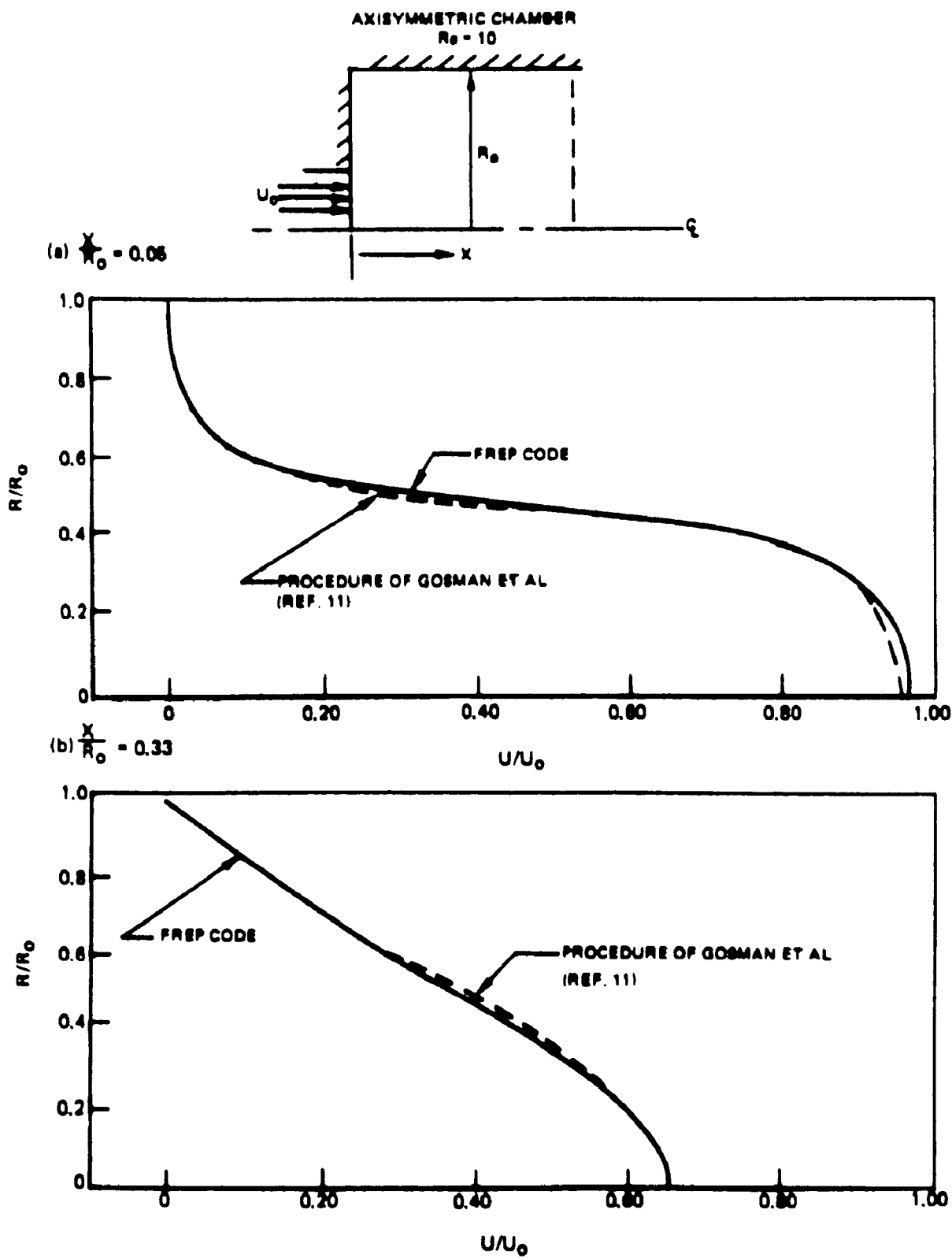
Any of nonlinear partial differential equations governing the flow in burners may be represented by the general partial differential equation developed previously, i.e.,

$$\begin{aligned} \sigma_{\phi} \left[ \frac{\partial}{\partial x} \left( \phi \frac{\partial \psi}{\partial r} \right) - \frac{\partial}{\partial r} \left( \phi \frac{\partial \psi}{\partial x} \right) \right] - \frac{\partial}{\partial x} \left[ b_{\phi_1} r \frac{\partial C_{\phi\phi}}{\partial x} \right] \\ - \frac{\partial}{\partial r} \left[ b_{\phi_2} r \frac{\partial C_{\phi\phi}}{\partial r} \right] + r d_{\phi} = 0 \end{aligned} \quad (11)$$

where the coefficients have been tabulated in TABLE I for each of the dependent variables,  $\phi$ , under consideration. It should be noted that the stream function equation serves as an auxiliary equation relating vorticity and velocity and is not solved alone sequentially in the general manner to be described. For solution the stream function is solved simultaneously with the vorticity equation. For the general numerical solution to Eq. (11) a finite-difference approximation is employed based on a three-point central differencing formula (see Fig. 3 for description of five-point molecule employed in this study).



## COMPUTED VELOCITY DISTRIBUTIONS



The difference analogue to Eq. (11) is written:

$$\begin{aligned}
 -C_{i+1,j} \phi_{i+1,j} \rightarrow C_{i-1,j} \phi_{i-1,j} - C_{i,j+1} \phi_{i,j+1} \\
 - C_{i,j-1} \phi_{i,j-1} + C_{ij} \phi_{ij} + \frac{d\phi}{b\phi} = 0
 \end{aligned} \tag{71}$$

where the pseudo-linear coefficients are defined as

$$\begin{aligned}
 C_{i+1,j} = \left\{ \left[ C_{x2}(1) + \left( \frac{C_{x1}(1)}{b_{\phi r}} \right) \left( \frac{\partial b_{\phi r}}{\partial x} \right) \right]_{ij} \right. \\
 \left. C_{\phi_{i+1,j}} - \left( \frac{a_{\phi} C_{x1}(1)}{b_{\phi r}} \right)_{ij} \left( \frac{\partial \psi}{\partial r} \right)_{ij} \right\}
 \end{aligned} \tag{72}$$

$$\begin{aligned}
 C_{i-1,j} = \left\{ \left[ C_{x2}(3) - \left( \frac{C_{x1}(3)}{b_{\phi r}} \right) \left( \frac{\partial b_{\phi r}}{\partial x} \right) \right]_{ij} \right. \\
 \left. C_{\phi_{i-1,j}} + \left( \frac{a_{\phi} C_{x1}(3)}{b_{\phi r}} \right)_{ij} \left( \frac{\partial \psi}{\partial r} \right)_{ij} \right\}
 \end{aligned} \tag{73}$$

$$\begin{aligned}
 C_{i,j+1} = \left\{ \left[ C_{y2}(1) + \left( \frac{C_{y1}(1)}{b_{\phi r}} \right) \left( \frac{\partial b_{\phi r}}{\partial r} \right) \right]_{ij} \right. \\
 \left. C_{\phi_{i,j+1}} + \left( \frac{a_{\phi} C_{y1}(1)}{b_{\phi r}} \right)_{ij} \left( \frac{\partial \psi}{\partial x} \right)_{ij} \right\}
 \end{aligned} \tag{74}$$

$$C_{i,j-1} = \left\{ \left[ C_{y2}(3) - \left( \frac{C_{y1}(3)}{b_{\phi r}} \right) \left( \frac{\partial b_{\phi r}}{\partial r} \right) \right]_{ij} \right. \\ \left. C_{\phi i,j-1} - \left( \frac{a_{\phi} C_{y1}(3)}{b_{\phi r}} \right) \left( \frac{\partial \psi}{\partial x} \right)_{ij} \right\} \quad (75)$$

$$C_{ij} = C_{xij} + C_{rij} = \left\{ \left[ C_{x2}(2) - \left( \frac{C_{x1}(2)}{b_{\phi r}} \right) \left( \frac{\partial b_{\phi r}}{\partial x} \right) \right]_{ij} C_{\phi ij} \right. \\ \left. + \left( \frac{a_{\phi} C_{x1}(2)}{b_{\phi r}} \right)_{ij} \left( \frac{\partial \psi}{\partial r} \right)_{ij} \right\} + \left\{ \left[ C_{y2}(2) - \left( \frac{C_{y1}(2)}{b_{\phi r}} \right) \left( \frac{\partial b_{\phi r}}{\partial r} \right) \right]_{ij} \right. \\ \left. C_{\phi ij} - \left( \frac{a_{\phi} C_{y1}(2)}{b_{\phi r}} \right)_{ij} \left( \frac{\partial \psi}{\partial x} \right)_{ij} \right\} \quad (76)$$

and the generalized coefficient arrays,  $C_{x1}$ ,  $C_{x2}$ ,  $C_{y1}$ , and  $C_{y2}$ , which are formulated to allow for nonuniform grid spacing, are defined according to the following relationships:

$$C_{x1}(1) = \Delta x_1 / \Delta x_2 (\Delta x_1 + \Delta x_2) \\ C_{x1}(2) = (\Delta x_2 - \Delta x_1) / \Delta x_1 \Delta x_2 \\ C_{x1}(3) = \Delta x_2 / \Delta x_1 (\Delta x_1 + \Delta x_2) \\ C_{x2}(1) = 2 / \Delta x_2 (\Delta x_1 + \Delta x_2) \\ C_{x2}(2) = 2 / \Delta x_1 \Delta x_2 \\ C_{x2}(3) = 2 / \Delta x_1 (\Delta x_1 + \Delta x_2) \quad (77)$$

and

$$\begin{aligned}
 \text{Cyl}(1) &= \Delta r_1 / \Delta r_2 (\Delta r_1 + \Delta r_2) \\
 \text{Cyl}(2) &= (\Delta r_2 - \Delta r_1) / \Delta r_1 \Delta r_2 \\
 \text{Cyl}(3) &= \Delta r_2 / \Delta r_1 (\Delta r_1 + \Delta r_2) \\
 \text{Cy2}(1) &= 2 / \Delta r_2 (\Delta r_1 + \Delta r_2) \\
 \text{Cy2}(2) &= 2 / \Delta r_1 \Delta r_2 \\
 \text{Cy2}(3) &= 2 / \Delta r_1 (\Delta r_1 + \Delta r_2)
 \end{aligned} \tag{78}$$

where

$$\begin{aligned}
 \Delta x_1 &= x_{ij} - x_{i-1,j} \\
 \Delta x_2 &= x_{i+1,j} - x_{ij}
 \end{aligned} \tag{79}$$

and

$$\begin{aligned}
 \Delta r_1 &= r_{ij} - r_{ij-1} \\
 \Delta r_2 &= r_{ij+1} - r_{ij}
 \end{aligned} \tag{80}$$

To numerically solve Eq. (71), an initial guess is made for  $\phi$  and an iterative field relaxation procedure is applied in which the governing set of residual difference equations, written for each node in the field, are solved implicitly by the ADI algorithm. In this manner, the residuals throughout the field are relaxed simultaneously at each iteration, a factor contributing greatly to the efficiency of the method. For development of the residual difference equations, it is convenient to introduce the residual,  $R_\phi$ , which can be written at the  $n^{\text{th}}$  iteration as

$$R\phi_{ij}^n = -C_{i+1,j}^n \phi_{i+1,j}^n - C_{i-1,j}^n \phi_{i-1,j}^n - C_{i,j+1}^n \phi_{i,j+1}^n - C_{i,j-1}^n \phi_{i,j-1}^n + C_{ij}^n \phi_{ij}^n + \left(\frac{d\phi}{b\phi}\right)_{ij}^n \quad (81)$$

For solution to Eq. (71) it is seen that it is necessary to reduce the residuals, defined by Eq. (81), to some sufficiently small value at all points in the field. For this purpose, appropriate adjustments are made to the representative dependent variable,  $\phi_{ij}$ , at all grid nodes simultaneously aimed at reducing all the residuals in the field to zero. This procedure is repeated at each iteration level until convergence is reached. The iteration formula employed in the iteration process is based on the following "chain rule" representation:

$$dR\phi_{ij}^n = \left(\frac{\partial R\phi_{ij}}{\partial \phi_{i-1,j}}\right)^n d\phi_{i-1,j}^n + \left(\frac{\partial R\phi_{ij}}{\partial \phi_{i+1,j}}\right)^n d\phi_{i+1,j}^n + \left(\frac{\partial R\phi_{ij}}{\partial \phi_{i,j+1}}\right)^n d\phi_{i,j+1}^n + \left(\frac{\partial R\phi_{ij}}{\partial \phi_{i,j-1}}\right)^n d\phi_{i,j-1}^n + \left(\frac{\partial R\phi_{ij}}{\partial \phi_{ij}}\right)^n d\phi_{ij}^n + \Phi_{ij}^n \quad (82)$$

where the partial derivatives are computed from Eq. (81) as

$$\begin{aligned} \left(\frac{\partial R\phi_{ij}}{\partial \phi_{i+1,j}}\right)^n &= -C_{i+1,j}^n \\ \left(\frac{\partial R\phi_{ij}}{\partial \phi_{i-1,j}}\right)^n &= -C_{i-1,j}^n \\ \left(\frac{\partial R\phi_{ij}}{\partial \phi_{i,j+1}}\right)^n &= -C_{i,j+1}^n \\ \left(\frac{\partial R\phi_{ij}}{\partial \phi_{i,j-1}}\right)^n &= -C_{i,j-1}^n \\ \left(\frac{\partial R\phi_{ij}}{\partial \phi_{ij}}\right)^n &= C_{ij}^n \end{aligned} \quad (83)$$



Equation (82) represents a set of finite-difference relaxation equations which are solved to advance the solution to the  $(n+1)$  iteration level. The term  $\Phi_{ij}^n$  represents a collection of terms appearing because the coefficients depend implicitly on  $\phi$  and because flow variables other than the dependent variable may induce changes in the residual. Since the values of  $\Phi_{ij}^n$  are not initially known, Eq. (82) is solved by a two-step procedure which is a generalization of the well-known secant method for finding roots of transcendental algebraic equations. During the first, or predictor step, intermediate values of the dependent variable  $\phi_{ij}$ , denoted  $\phi_{ij}^*$ , are computed from Eq. (82) by neglecting  $\Phi_{ij}^n$  altogether. The information gained from the predictor step is then extrapolated to determine  $\Phi_{ij}^n$  which is then employed to determine  $(n+1)$  level iteration values for the dependent variable in the second, or connector, step. Thus, writing  $d_{ij}^n = \phi_{ij}^* - \phi_{ij}^n$  and employing Eq. (71), the relaxation formula becomes for the predictor step:

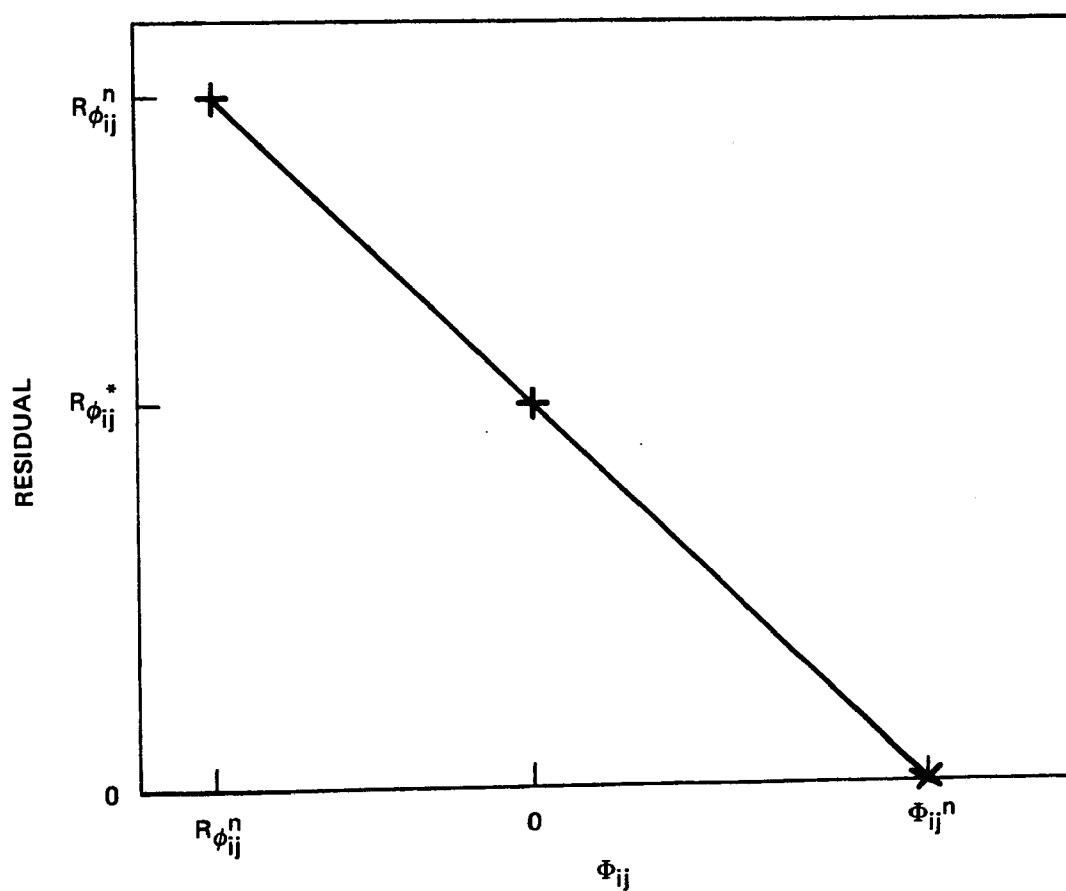
$$\begin{aligned} -C_{i+1,j}^n \phi_{i+1,j}^* - C_{i-1,j}^n \phi_{i-1,j}^* - C_{i,j+1}^n \phi_{i,j+1}^* \\ - C_{i,j-1}^n \phi_{i,j-1}^* + C_{ij}^n \phi_{ij}^* = - \left( \frac{d\phi}{b\phi} \right)_{ij}^n \end{aligned} \quad (84)$$

With Eq. (84) written at each grid node, a system of linear equations is obtained which is solved by an ADI algorithm, described below. From solution of Eq. (84), the intermediate value of the dependent variables,  $\phi_{ij}^*$ , are determined. Once these values are known, intermediate values for the coefficients in Eq. (71) are computed and then employed for computing the residual,  $R\phi_{ij}$ . Sufficient information is now available to compute values for  $\Phi_{ij}^n$  (in advance) for displacement from the  $n$ -level to the  $(n+1)$  level by linear extrapolation of known values of the residual at the  $n$ -level and  $*$ -levels. For example, if one considers first a zero displacement in  $\phi$  at the  $n$ -level, so that  $d\phi_{ij}^n = 0$ , it follows that the residual computed from Eq. (71) would just be  $R\phi_{ij}$  and, hence, by Eq. (81),  $\Phi_{ij}^n = R\phi_{ij}$ . If a second displacement is now considered from the  $n$ -level to the  $*$ -level, it is known from the predictor step that the residual is  $R\phi_{ij}^*$ , and the value for  $\Phi_{ij}^n$  for this case was considered to be zero. Hence, employing a secant extrapolation (see Fig. 7) the desired values for  $\Phi_{ij}^n$  to be employed in the corrector step are given by

$$\Phi_{ij}^n = R\phi_{ij}^n / (1 - R\phi_{ij}^n / R\phi_{ij}^*) \quad (85)$$

**EXTRAPOLATION PROCEDURE**  
**COUPLING AND LINEARIZATION TERM ,  $\Phi_{ij}^n$**

(SEE EQ. (63) )



Hence, in the second step of the procedure, values for  $\phi_{ij}^{n+1}$  are computed from the following expression (which is identical to Eq. (84) with exception of the  $\Phi_{ij}^n$  term) derived from Eq. (71)

$$\begin{aligned} & -C_{i+1,j}^n \phi_{i+1,j}^{n+1} - C_{i-1,j}^n \phi_{i-1,j}^{n+1} - C_{ij+1}^n \phi_{i,j+1}^{n+1} \\ & - C_{ij-1}^n \phi_{ij-1}^{n+1} + C_{ij}^n \phi_{ij}^{n+1} = - \left( \frac{d\phi}{b\phi} \right)_{ij}^n - \Phi_{ij}^n \end{aligned} \quad (86)$$

where Eq. (85) is employed to determine  $\Phi_{ij}^n$ .

$$\begin{aligned} & C_{i+1,j}^n \phi_{i+1,j}^{n+1} - C_{i-1,j}^n \phi_{i-1,j}^{n+1} - C_{ij+1}^n \phi_{i,j+1}^{n+1} \\ & - C_{ij-1}^n \phi_{ij-1}^{n+1} + C_{ij}^n \phi_{ij}^{n+1} = - \left( \frac{d\phi}{b\phi} \right)_{ij}^n - \Phi_{ij}^n \end{aligned} \quad (67)$$

where Eq. (67) is employed to determine  $\Phi_{ij}^n$ .

The foregoing two-step implicit relaxation technique, while apparently complicated, is in reality quite straightforward in application. For example, in a hypothetical case in which the values of the coefficients,  $C_{ij}$ , are not dependent on  $\phi_{ij}$ , the  $\Phi_{ij}^n$  term is identically zero and the exact solution is obtained in one iteration (the first half-step of this iteration can be omitted since the  $\phi_{ij}^n$  is known). The main advantage of the new technique is that during an iteration all the residuals in the field are reduced to zero simultaneously and, at the same time, the effects of nonlinearity and coupling can be taken into account via the  $\Phi_{ij}^n$  term. Moreover, unlike methods which employ point by point iteration, the number of iterations required for convergence should be more or less independent of the number of grid points used. Thus the gain in efficiency relative to point methods is increased as additional grid points are added.

As a final note, it should be mentioned that, in the original application of the two-step procedure under this contract, certain difficulties were experienced in maintaining computational efficiency in cases involving high Reynolds numbers and in applying vorticity boundary conditions. In the case of the vorticity boundary conditions, because implicit values of vorticity along certain boundaries were not known a priori as required, an extrapolation technique became necessary which detracted from the efficiency of the

procedure. In the high Reynolds number cases, loss of efficiency was determined to be due to the fact that coupling and linearization effects enter only through the corrector step; consequently, at high Reynolds numbers, when coupling and linearization effects are more significant, the predictor step is not particularly accurate and the efficiency of the procedure was found to suffer.

The code was subsequently developed to correct the computational efficiency problems referred to above by solving the vorticity and stream function equations simultaneously as a coupled pair. For example, the coupled solution of the vorticity and stream function equations permits the vorticity boundary conditions to be incorporated as part of the solution procedure, thereby eliminating the extrapolation procedure altogether. In addition, because of the coupling, it became possible to include extra stream function implicit terms in the vorticity finite-difference residual equations (see Eq. (84)). The addition of these terms improved the imbalance between the predictor and corrector steps of the solution procedure at high Reynolds numbers because it added coupling terms in the predictor step. Thus, by solving the vorticity and stream function as a coupled pair, refinements to the numerical code are implemented which improve the efficiency of the computational procedure and the range of flow variables to which it can be applied.

### III-C. ADI SOLUTION PROCEDURE

In order to iterate to the solution of the residual finite-difference analogue to the governing elliptic equations representing the flow in a furnace (Eq. (71)) a system of linear algebraic difference equations must be solved. The difference equations requiring solution are of the general form (see Eq. (84) or Eq. (86)):

$$\begin{aligned}
 & - C_{i-1,j}^n \phi_{i-1,j}^{n+1} + C_{xij}^n \phi_{ij}^{n+1} - C_{i+1,j}^n \phi_{i+1,j}^{n+1} \\
 & - C_{ij+1}^n \phi_{i,j+1}^{n+1} + C_{rij}^n \phi_{ij}^{n+1} - C_{i,j-1}^n \phi_{i,j-1}^{n+1} = f_{ij}^n
 \end{aligned} \tag{87}$$

where  $i, j$  are grid nodes and  $n$  is the residual iteration level. Solution of a pentadiagonal matrix is required to solve Eq. (87) in this form, and in view of the special structure of this pentadiagonal matrix the highly efficient ADI algorithm of Peaceman and Rachford (Ref. 44) can be used. The Peaceman-Rachford algorithm solves the system of equations iteratively and at each

iteration reduces the pentadiagonal matrix to a tridiagonal form which is easily and efficiently solved by Gaussian elimination. To implement the ADI procedure, it is convenient to separate the horizontal from the vertical differencing terms in Eq. (87) in the following two ways

$$\begin{aligned}
 & -C_{i-1,j}^n \phi_{i-1,j}^{n+1} + C_{xij}^n \phi_{ij}^{n+1} - C_{i+1,j}^n \phi_{i+1,j}^{n+1} + \rho \phi_{ij}^{n+1} \\
 & = \rho \phi_{ij}^{n+1} + C_{ij-1}^n \phi_{ij-1}^{n+1} - C_{rij}^n \phi_{ij}^{n+1} + C_{i,j+1}^n \phi_{i,j+1}^{n+1} + f_{ij}^n
 \end{aligned} \tag{88}$$

and

$$\begin{aligned}
 & C_{i,j-1}^n \phi_{i,j-1}^{n+1} + C_{rij}^n \phi_{ij}^{n+1} - C_{i,j+1}^n \phi_{i,j+1}^{n+1} + \rho \phi_{ij}^{n+1} = \rho \phi_{ij}^{n+1} \\
 & + C_{i-1,j}^n \phi_{i-1,j}^{n+1} - C_{xij}^n \phi_{ij}^{n+1} + C_{i+1,j}^n \phi_{i+1,j}^{n+1} + f_{ij}^n
 \end{aligned} \tag{89}$$

where  $\rho$  may be regarded as a psuedo time step parameter referred to as the "iteration parameter" or the "acceleration parameter" (see section on ITERATION PARAMETER). The Peaceman-Rachford ADI iteration method solves the set of equations represented by Eq. (87) by solving Eqs. (88) and (89) alternately by sets of rows or columns until convergence is reached. Accordingly, Eqs. (88) and (89) are written

$$\begin{aligned}
 & \left\{ -C_{i-1,j}^n \phi_{i-1,j}^{n+1} + (C_{xij}^n + \rho) \phi_{ij}^{n+1} - C_{i+1,j}^n \phi_{i+1,j}^{n+1} \right\}^{M+1} \\
 & = \left\{ C_{ij-1}^n \phi_{ij-1}^{n+1} - (C_{rij}^n + \rho) \phi_{ij}^{n+1} + C_{i,j+1}^n \phi_{i,j+1}^{n+1} \right\}^M + f_{ij}^n
 \end{aligned} \tag{90}$$

$$\begin{aligned}
 & \left\{ -C_{i,j-1}^n \phi_{i,j-1}^{n+1} + (C_{rij}^n + \rho) \phi_{ij}^{n+1} - C_{i,j+1}^n \phi_{i,j+1}^{n+1} \right\}^{M+2} \\
 & = \left\{ C_{i-1,j}^n \phi_{i-1,j}^{n+1} - (C_{xij}^n + \rho) \phi_{ij}^{n+1} + C_{i+1,j}^n \phi_{i+1,j}^{n+1} \right\}^{M+1} + f_{ij}^n
 \end{aligned} \tag{91}$$

where M represents the ADI iteration index. Thus, Eq. (90) is employed to advance the solution to the (M+1) iteration level followed by Eq. (91) which is used for advancement from the (M+1) to the (M+2) iteration level. Values at the (M-1) iteration level are presumed known either from the previous iteration, or from an initial guess. Solution to Eqs. (90) or (91) is easily and efficiently obtained by employing an algorithm for solving tridiagonal matrices.

Convergence is determined in the ADI procedure by the following test

$$\left\{ \frac{[\phi_{ij}]^{n+1, M} - [\phi_{ij}]^{n+1, M-1}}{[\phi_{ij}]^{n+1, M}} \right\}_{\text{MAX}} \leq \epsilon_1 \quad (92)$$

which dictates the maximum fractional change of  $\phi$  which is allowed in the field must not exceed a prescribed value,  $\epsilon_1$ , which is typically in the range, 0.001 to 0.005. An alternate criterion is sometimes employed when the value of  $\phi$  at a particular node is very small relative to surrounding values. In this case the following formula is employed

$$\left\{ \frac{[\phi_{ij}]^{n+1, M} - [\phi_{ij}]^{n+1, M-1}}{[\phi_{ij, \text{MAX}}]^{n+1, M}} \right\}_{\text{MAX}} \leq \epsilon_2 \quad (93)$$

where the change in the variable has been divided by the maximum value in the field. Typically,  $\epsilon_2$  is set in the range 0.0001 to 0.00005.

#### III-D. ITERATION PARAMETERS

The rate of convergence of the ADI procedure is very sensitive to the choice of acceleration parameters,  $\rho$ , and improper values will very likely result in divergent behavior. Unfortunately, little is known of the correct values for the acceleration parameter to be applied to the coupled nonlinear equations requiring solution for the present problem and information must be inferred from knowledge gained in simpler linear systems. The parameters employed by Peaceman and Rachford for solving Laplace's equation are defined according to

$$\rho_j = b (a/b)^{(2j-1)/2m} \quad j=1,2,\dots,m \quad (94)$$

where  $a$  and  $b$  represent minimum and maximum eigenvalues of the tridiagonal matrix, and  $m$  refers to the number of parameters to be employed. The rate of convergence of ADI methods can be appreciably increased by the application of several iteration parameters which are used successively in cyclic order. Estimates of optimum choice of the number of parameters to be used can be determined (Ref. 46) by finding the smallest integer  $m$  such that

$$(\delta)^{2m} \leq \frac{a}{b} \quad (95)$$

where

$$\delta = \sqrt{2} - 1 = 0.414 \quad (96)$$

This procedure for evaluating iteration parameters and determining the optimum number to be employed was not found to be completely satisfactory in the computational procedure, for cases where convection and source terms in the governing differential equation were large relative to the diffusion terms. Accordingly, a theoretical analysis was undertaken wherein a simple time-dependent linear analogue of the governing differential equations was investigated and compared against the analytical solution to the diffusion equation, for which the parameters are known from Eq. (94), for the purpose of obtaining some insight into appropriate iteration parameters to be employed. Consider the following linear differential equation

$$\frac{\partial^2 \phi}{\partial x^2} + 2a \frac{\partial \phi}{\partial x} + \frac{f}{\alpha} = \frac{1}{\alpha} \frac{\partial \phi}{\partial t} \quad (97)$$

For boundary and initial conditions specified as

$$\begin{aligned}\phi(x, t_0) &= \phi_i \\ \phi(x_0, t) &= \phi_0 \\ \phi(x, t) &= \phi\end{aligned}\tag{98}$$

solution becomes

$$\begin{aligned}\phi - \phi_0 &= (\phi_i - \phi_0) \operatorname{ERF} \left[ \frac{x - x_0}{\sqrt{4\alpha(t-t_0)}} \right] \\ \exp \left[ -\alpha(x-x_0) - \alpha^2 \alpha(t-t_0) \right] + f(t-t_0)\end{aligned}\tag{99}$$

The iteration parameters can be shown to be related to the time step in the following manner (by differencing Eq. (97) and comparing against Eq. (88))

$$\rho = \frac{(x-x_0)^2}{(t-t_0)}\tag{100}$$

Employing Eq. (100), Eq. (99) can be written

$$\Delta\phi = \Delta\phi_0 \operatorname{ERF} \sqrt{\frac{\rho}{4\alpha}} \exp \left[ -\alpha\Delta x \left( 1 + \frac{\alpha\alpha\Delta x}{\rho} \right) \right] + \frac{f\Delta x}{\rho}\tag{101}$$

where

$$\begin{aligned}\Delta\phi &= \phi - \phi_0 \\ \Delta\phi_0 &= \phi_i - \phi_0 \\ \Delta x &= x - x_0\end{aligned}\tag{102}$$



Three cases can now be considered in order to provide insight to appropriate values for  $\rho$  by considering the governing equations to be either diffusion dominated, convection dominated, or source dominated.

CASE 1. DIFFUSION DOMINATED - If the diffusion terms in the governing differential equation are much larger than the convection source terms, Eq. (97) effectively reduces to the diffusion equation

$$\frac{\partial^2 \phi}{\partial x^2} = \frac{1}{\alpha} \frac{\partial \phi}{\partial t} \quad (103)$$

with solution

$$\Delta \phi = \Delta \phi_0 \operatorname{ERF} \sqrt{\frac{\rho}{4\alpha}} \quad (104)$$

where satisfactory values for  $\rho$  are given by Eq. (94) as determined by Peaceman and Rachford:

$$\rho = b (a/b)^{(2j-1)/2m} \quad j = 1, 2, \dots, m \quad (94)$$

CASE 2. CONVECTION DOMINATED - For the case where the governing equations are convection dominated the governing equation, Eq. (97), is written

$$2\alpha \frac{\partial \phi}{\partial x} = \frac{1}{\alpha} \frac{\partial \phi}{\partial t} \quad (105)$$

with solution

$$\Delta \phi = \Delta \phi_0 \exp \left[ -\alpha \Delta x \left( 1 + \frac{\alpha \Delta x}{\rho} \right) \right] \quad (106)$$

which is solved for  $\rho$ :

$$\rho = \frac{-\alpha(a\Delta x)^2}{\left[ a\Delta x + \ln\left(\frac{\Delta\phi}{\Delta\phi_0}\right) \right]} \quad (107)$$

CASE 3. SOURCE TERM - For the source dominated case, the governing equation, Eq. (97), is written

$$\frac{\partial\phi}{\partial t} = f \quad (108)$$

with solution

$$\frac{\Delta\phi}{\Delta\phi_0} = 1 + \frac{f\Delta x^2}{\Delta\phi_0\rho} \quad (109)$$

which when solved for  $\rho$  becomes

$$\rho = \frac{f\Delta x^2}{(\Delta\phi - \Delta\phi_0)} \quad (110)$$

By comparing Eq. (97) against the general elliptic partial differential equation being solved under this investigation the following relationships can be deduced

$$\alpha = \nu \quad (111)$$

$$\begin{aligned}
a &\approx -\frac{1}{2} \left[ \frac{a\phi}{b\phi r c\phi} \frac{\partial \psi}{\partial r} - \frac{1}{b\phi r} \frac{\partial b\phi r}{\partial x} \right] \\
&\approx \frac{1}{2} \left[ \frac{a\phi}{b\phi r c\phi} \frac{\partial \psi}{\partial x} + \frac{1}{b\phi r} \frac{\partial b\phi r}{\partial r} \right]
\end{aligned} \tag{112}$$

$$f = \frac{-\nu d\phi}{b\phi c\phi} \tag{113}$$

By employing Eqs. (111) through (113) it is possible to determine whether the governing elliptic partial differential equation is diffusion, convection, or source term dominated. Depending on the case, Eq. (94), (107), or (110), respectively, is employed to evaluate the acceleration parameter. To solve for  $\rho$  in these three equations, however, requires knowledge of  $\Delta\phi_0$  and  $\Delta\phi$  ( $\Delta X$  is taken to be a representative grid spacing). For this purpose, Eq. (104) can be employed ( $\rho$  and  $\alpha$  are known for the diffusion dominated case from Eqs. (94) and (111), respectively). Thus,

$$\frac{\Delta\phi}{\Delta\phi_0} = \left( \text{ERF} \sqrt{\frac{\rho}{4\alpha}} \right) \text{ DIFFUSION DOMINATED} \tag{114}$$

Equation (114) provides sufficient information to determine  $\rho$  in Eqs. (94) or (107); however, to determine  $\rho$  in the source dominated case, Eq. (110), the ratio  $\Delta\phi/\Delta\phi_0$  is not sufficient since values for both  $\Delta\phi_0$  and  $\Delta\phi$  are required. In this case, the assumption is made that across a grid spacing a one percent change in the function is allowable in the given time step. Thus,

$$\Delta\phi = 0.01 \tag{115}$$

and  $\Delta\phi_0$  can be computed from Eq. (114).

### III-E. ITERATIVE PROCEDURE AND ORDER OF SOLUTION

Equations solved by the computational procedure under this investigation include: vorticity, stream function, stagnation enthalpy, fuel mass fraction, swirl velocity, two radiant heat transfer functions, and nitric oxide mass fraction. Pressure, temperature, density, viscosity, other species concentrations, and other flow variables are deduced from these dependent variables. While solving these equations, in order to remain within a UNIVAC 1108 computer storage limitations, it was necessary to transfer data on and off auxiliary storage facilities. Consequently, the above equations were solved within the program in three sets, comprising groups of five or less. The first group solved in the computational procedure consists of vorticity, stream function, stagnation enthalpy, and fuel mass fraction, in that order. The second and third groups consist of the following equations: swirl velocity and two radiant heat transfer equations in the second group, and the nitric oxide mass fraction equation in the third group.

Starting with an initial guess for all flow properties, a cycle of iterative sequence of operations begins with computation of residuals for each equation to be solved (with exception of stream function equation). For the predictor step, iteration is initiated by solving Eq. (84) for all the dependent variables by employing the ADI solution procedure. When convergence is reached for all the equations, the secant extrapolation is implemented to evaluate corrections for nonlinearity and coupling which were neglected in the predictor step, but which are required for execution of the corrector step. The corrector step is then implemented by solving Eq. (85) by the ADI method to determine updated values for all the dependent variables. The nonlinearity and coupling correction is introduced through the variable,  $\Phi_{ij}^n$ . As stream function is considered an auxiliary equation, it is coupled with the vorticity equation and solved simultaneously with the vorticity in the corrector step as in the predictor step by employing Eq. (84). Auxiliary relationships are then invoked to update pressure, temperature, density, viscosity, and other flow variables before start of the next iteration cycle. Convergence is determined by the following test, as in the ADI procedure

$$\left\{ \frac{\phi_{ij}^n - \phi_{ij}^{n-1}}{\phi_{ij}^n} \right\}_{\text{MAX}} \leq \epsilon \quad (116)$$

where  $\epsilon$  is of the order of 0.001 or less.

## SECTION IV

### RESULTS AND DISCUSSION

To validate the computational procedure comparisons were made with the nonreacting turbulent swirling jet flow of Chigier and Chervinsky (Ref. 46). In particular, it was recognized that for low and moderate degrees of inlet swirl Lilley (Ref. 20) had obtained very satisfactory comparisons with Chigier's data using a finite-difference boundary layer procedure together with the turbulence model detailed in II.B.1. As was mentioned previously, the appearance of a recirculation zone and the occurrence of large radial velocities with high degrees of inlet swirl velocity, made calculations using the boundary layer equations unacceptable in this flow regime. However, it was felt that predictions made using the FREP code should agree with Lilley's predictions (and the data) at low to moderate inlet swirl velocities. These comparisons were performed under a Corporate-sponsored program but were reported here in detail in view of their importance in validating the FREP code. To demonstrate the applicability of the FREP code to predict the flow field within a representative furnace, further comparisons were performed under the present contract with the data of Larson and Shoffstall (Ref. 47). Larson, et al., measured the mean velocity field in the turbulent swirling jet of a furnace both with and without combustion.

#### IV-A. COMPARISON WITH THE DATA OF CHIGIER, ET AL. (REF. 46)

In Ref. 46 Chigier, et al., report an experimental and theoretical investigation of the turbulent swirling jet. Subsequently, Lilley (Ref. 20) compared Chigier's measurements to predictions of the jet made using a turbulence model which he constructed together with a finite-difference procedure to integrate the boundary layer equations. For low and moderate degrees of swirl velocity the comparisons were very satisfactory and, consequently, it was decided to perform a similar set of comparisons with Chigier's data using the FREP code. Since the turbulence model was the same in both comparisons, good agreement between FREP code predictions and Lilley's predictions and, of course, the data, was expected. However, it became apparent in setting up the cases that detailed initial profiles at the inlet plane were not available to start the calculations and the subsequent behavior, in particular, the decay of the potential core region, was very sensitive to the choice of the initial profiles. In addition, it was not clear how Lilley had started his calculations, or what special procedure he used to calculate the potential core decay. As a result of these considerations, an alternate comparative scheme was adopted based on the similitary hypothesis.

Basically, the similarity hypothesis argues that for turbulent flow far from the orifice the jet properties would become invariant (similar) with streamwise direction when expressed in a certain coordinate system. Chigier, et al., (Ref. 46) investigated the similarity hypothesis and observed that when expressed  $\xi, \eta$  coordinates, where  $\xi$  is  $x + a$ ,  $a$  being the streamwise distance from the effective origin of the flow and  $\eta$  being  $r/(x+a)$ , then mean profile similarity was obtained after approximately 4 to 10 jet diameters of streamwise development. Accordingly, comparisons are presented in terms of the similarity variables for three degrees of inlet swirl velocity corresponding to a weak, intermediate, and strong coupling between the axial and rotational velocity fields. In all cases a reference position  $x_i$  was adopted downstream of which the flow could be considered to be similar. The subsequent decay of the axial velocity maximum,  $U_m$ , was expressed as a fraction of the axial velocity maximum at the reference location  $U_{m_i}$ , and similarly for the swirl velocity maximum  $W_m$ . The velocity decay in the streamwise direction is presented in terms of the ratio  $\xi_i/\xi$  for the axial component and  $(\xi_i/\xi)^2$  for the swirl component since Chigier indicated that on the basis of similarity the decay would be linear when expressed in this manner. The comparisons between the predictions of the FREP code and the data are presented in Figs. 8 through 16. A 28 x 20 grid was used in the computation and it can be seen that a very acceptable level of agreement between prediction and measurement has been obtained. For the high swirl case only at the last measuring station was the flow development approximately similar. However, it did appear for this high swirl case that the potential core region was negligible and that a comparison in real variables might be warranted. Such a comparison is shown in Fig. 17, where the axial development of the profile of the velocity vector is presented. Obviously, further refinements to the inlet profiles could have improved the comparison between prediction and measurement but that qualitatively the agreement is quite good. It was also evident from the results that with this high degree of swirl velocity the radial velocity component was quite large, nonnegligible, and insofar as the measurements are concerned, unknown.

#### IV-B. COMPARISON WITH THE DATA OF D. H. LARSON AND D. R. SHOFFSTALL (REF. 47)

Under EPA Contract No. 68-02-0216 with the Institute of Gas Technology, the flow field within a gas fired furnace has been mapped for both hot- and cold-flow conditions. With cold-flow two degrees of inlet swirl velocity were explored, designated minimum and high swirl. For the high swirl case a large recirculation zone formed downstream of the inlet. The hot-flow data were obtained by burning natural gas.

#### IV-B.1 Cold-flow comparisons

The comparisons between the predictions and the IGT measurements were, like the Chigier comparisons, also influenced by the unknowns in the inlet flow conditions. However, the details of the inlet flow are much more likely to influence the low swirl calculations than the high swirl comparisons, since with large swirl velocities there is very rapid intense mixing which tends to quickly eradicate the details of the inlet profiles. In this regard it is perhaps worth noting that the calculation domain could have been extended into the inlet pipe upstream of the influence of the expansion into the burner. At such an upstream location it would be presumably much easier to specify a set of reasonable pipe flow conditions from which to initiate the calculation. In view of the computer logic involved, for the present, all the calculations have been initiated at the burner entrance. In Fig. 18 a comparison between the measured and predicted axial velocity profiles in the turbulent jet with the minimum degree of inlet swirl velocity is given. In general, a very good degree of qualitative and quantitative comparison between measurement and prediction is shown, with the theory indicating slightly too slow a decay of the profile at the third and fourth measuring stations. In Fig. 19 a similar comparison is shown for the highly swirling case and it can be seen that although the inlet conditions have not been matched precisely the profiles in the recirculation zone are predicted remarkably well. In Fig. 20 the theoretical streamlines for the highly swirling case are presented and from it it is evident that close to the inlet the flow is changing very rapidly and in view of the streamline curvature the radial velocity component is obviously quite large. It should perhaps be mentioned at this point that the upper boundary condition applied for all of the comparisons shown so far was that the variable second derivative with respect to the radial direction was zero. This very weak boundary condition was applied in favor of going out a very large distance to a solid wall or as in the Chigier case to some distant location where the vorticity was zero.

#### IV-B.2 Hot-Flow Comparisons

In view of the difficulties associated with making measurements in hot flows only a very limited amount of aerodynamic data was obtained by Larson and Shoffstall (Ref. 47) for the burner considered here. In making the theoretical calculations it was assumed that the same inlet profile of fuel and air would be obtained as in the comparable cold flow case and the magnitude of the inlet fuel and air velocities were simply scaled to give the quoted fuel flow rate and overall stoichiometry. Insofar as the swirl component was concerned some doubt was expressed as to the behavior of the aluminum swirl generating blocks under hot flow conditions. As a consequence of this two calculations were performed, one with the same relative swirl distribution as in the cold flow case and the second with the swirl component

increased by 1.333. With the same relative swirl distribution, only a very small recirculation zone was obtained in the hot flow case; however, in the hot case the flow in the region where the cold flow recirculation zone had existed was of very low velocity, although not quite reversed. In the second case where the swirl distribution was scaled by 1.333 a much larger recirculation zone, similar in size to the cold flow recirculation zone, was obtained. Comparisons with the data have been made only for the higher swirl case.

Before proceeding to discuss the hot flow results, two points concerning the hot flow calculations should be made. The first of these was that, it was found beneficial to start the calculation from a cold flow solution and under-relax the temperature field during the first few iterations around the stream function - vorticity and the stagnation enthalpy equations. The under-relaxation consisted of taking some fraction of the computed local temperature together with one minus this fraction of the previous local temperature, to determine the current local temperature. A new density was then computed to be consistent with the under-relaxed local temperature. The fraction of the new temperature increased smoothly as the iteration proceeded until after five outer iterations round the entire system, the degree of under-relaxation was negligible.

As a second point it should be noted that in solving for the diffusion of nitric oxide, the nonequilibrium species production term in the governing equations,  $r_i$ , in Eq. (2), was nonnegligible and highly nonlinear. The incorporation of this  $r_i$  term, or indeed any source term  $d\phi$  containing the dependent variable, into the present computational framework was straightforward. To account for such a term, it is necessary in the development of the change in residual, Eq. (82), to allow for the contribution due to the rate of change of the source term  $d\phi/b\phi$  with the dependent variable  $\phi$ . This contribution is added to  $C_{ij}^n$  in Eq. (83), and the resulting linear system solved using FREP. At this point a new rate of change of  $d\phi/b\phi$  with dependent variable  $\phi$  is evaluated throughout the field and, if necessary, the linear system may be resolved. The process is repeated until the computed dependent variable does not change to within a specified tolerance. This process is obviously simply a variation of the Newton-Raphson method for solving nonlinear equations. For the calculation of the nitric oxide concentrations in the cases examined to date, the technique proved highly efficient.

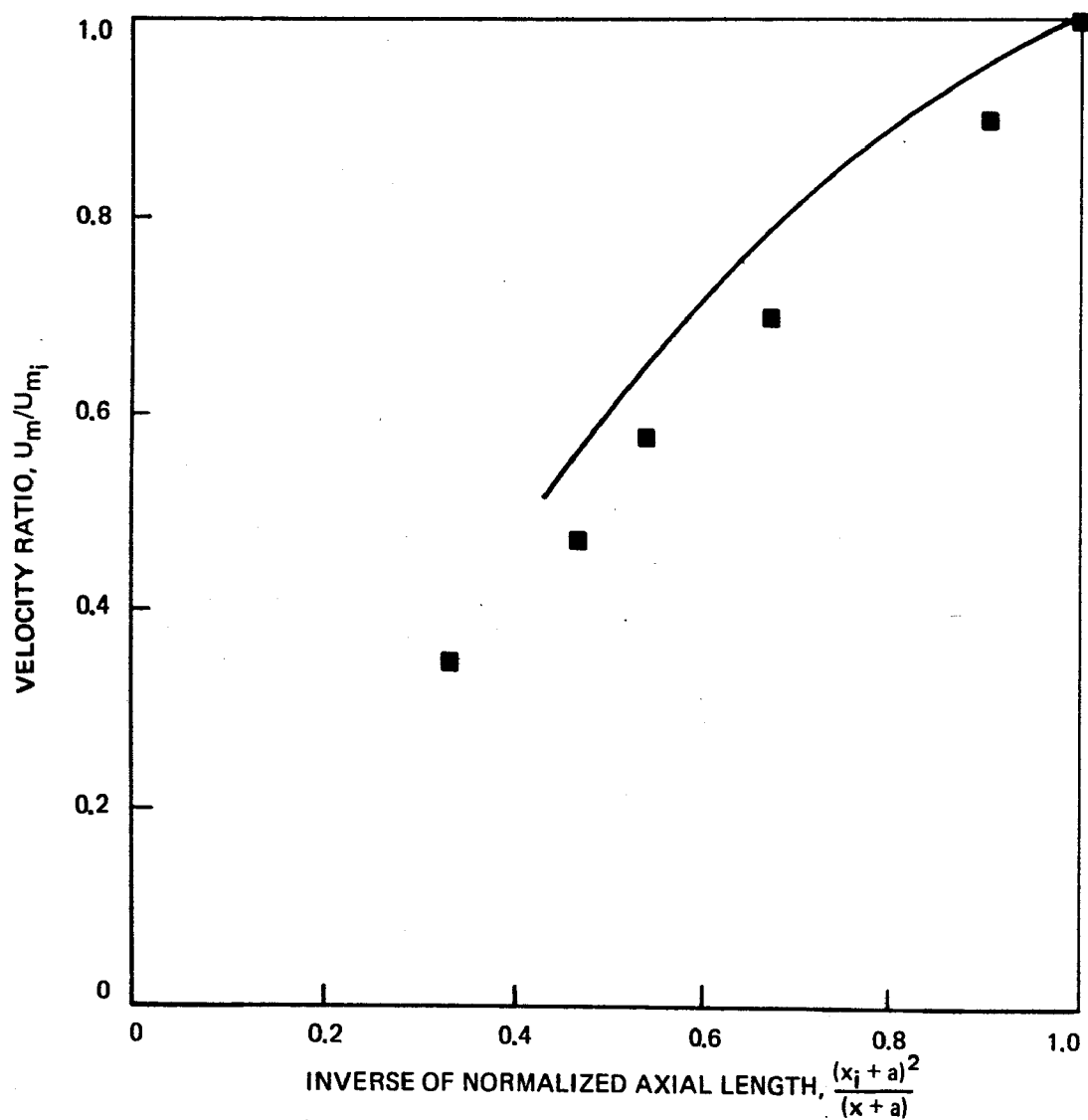


# A COMPARISON BETWEEN PREDICTED AND MEASURED AXIAL DECAY OF THE VELOCITY MAXIMUM IN A TURBULENT SWIRLING JET

MODERATELY SWIRLING JET,  $S = 0.134$

■ MEASUREMENTS OF CHIGIER (REF. 46)

— PREDICTION

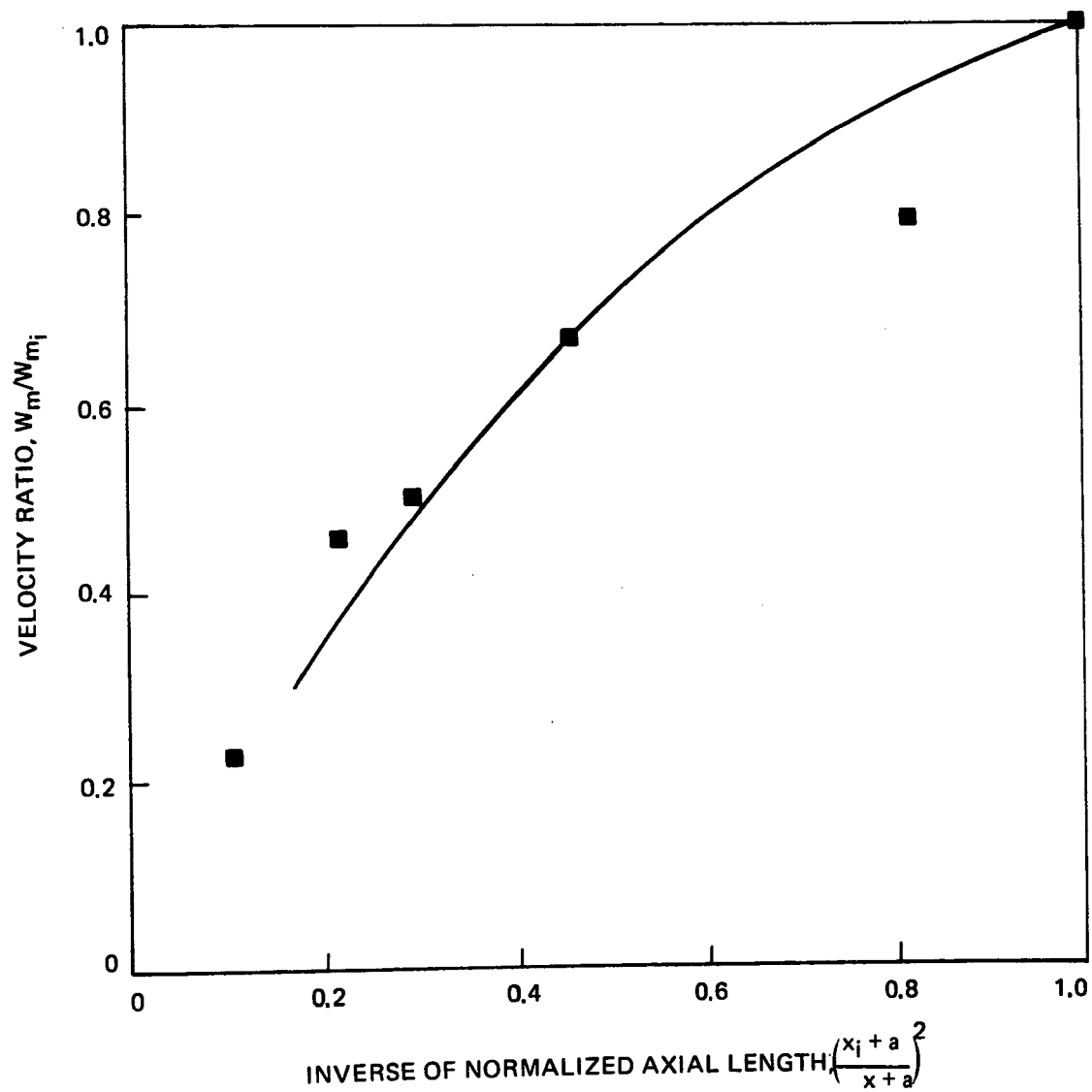


# A COMPARISON BETWEEN PREDICTED AND MEASURED AXIAL DECAY OF THE SWIRL VELOCITY MAXIMUM IN A TURBULENT SWIRLING JET

MODERATELY SWIRLING JET,  $S = 0.134$

■ MEASUREMENTS OF CHIGIER (REF. 46)

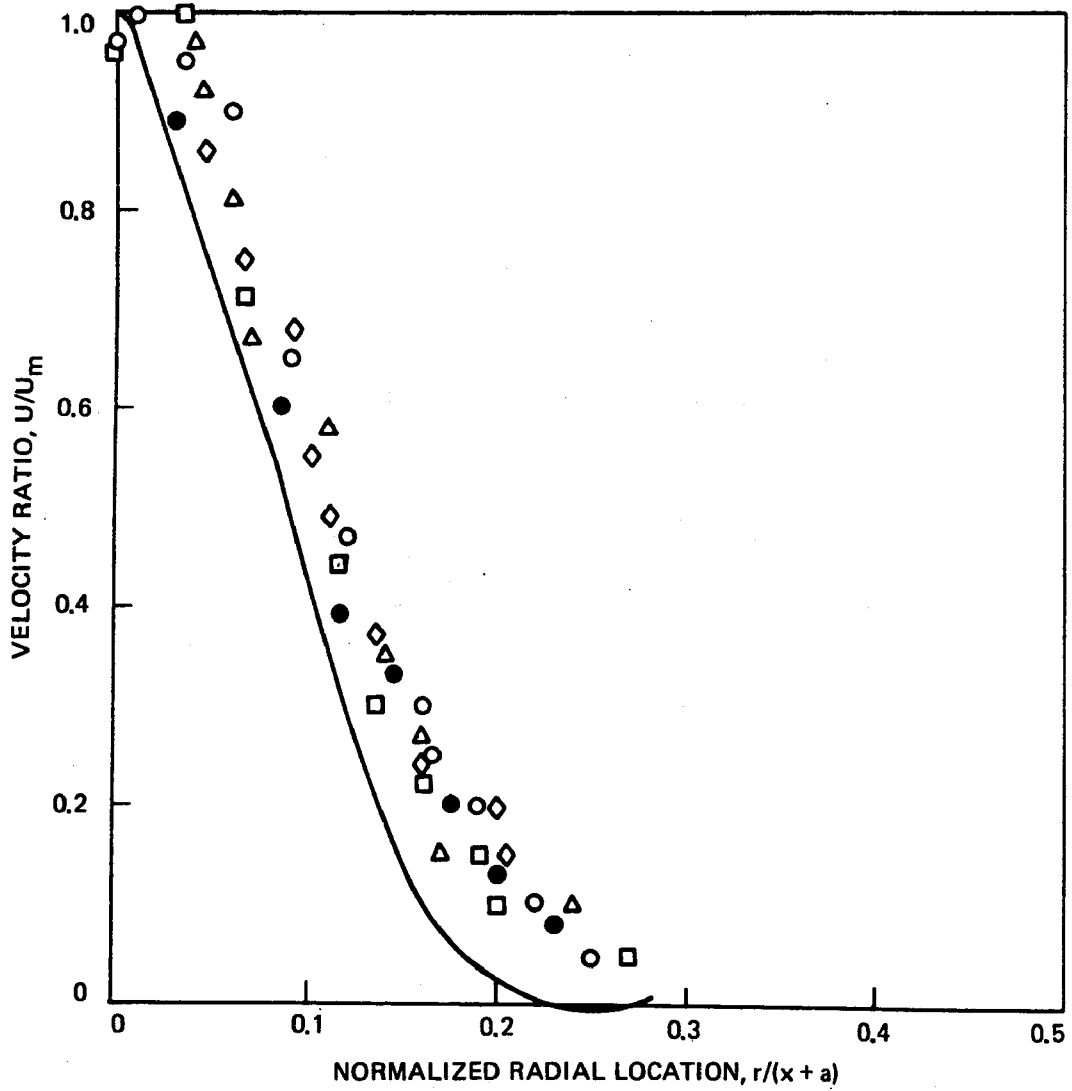
— PREDICTION



# COMPARISON BETWEEN THEORY AND MEASUREMENT OF THE MEAN VELOCITY PROFILE IN A TURBULENT SWIRLING JET

MODERATELY SWIRLING JET,  $S = 0.134$

○ □ △ ◇ ● MEASUREMENTS OF CHIGIER (REF. 46)  
— PREDICTION

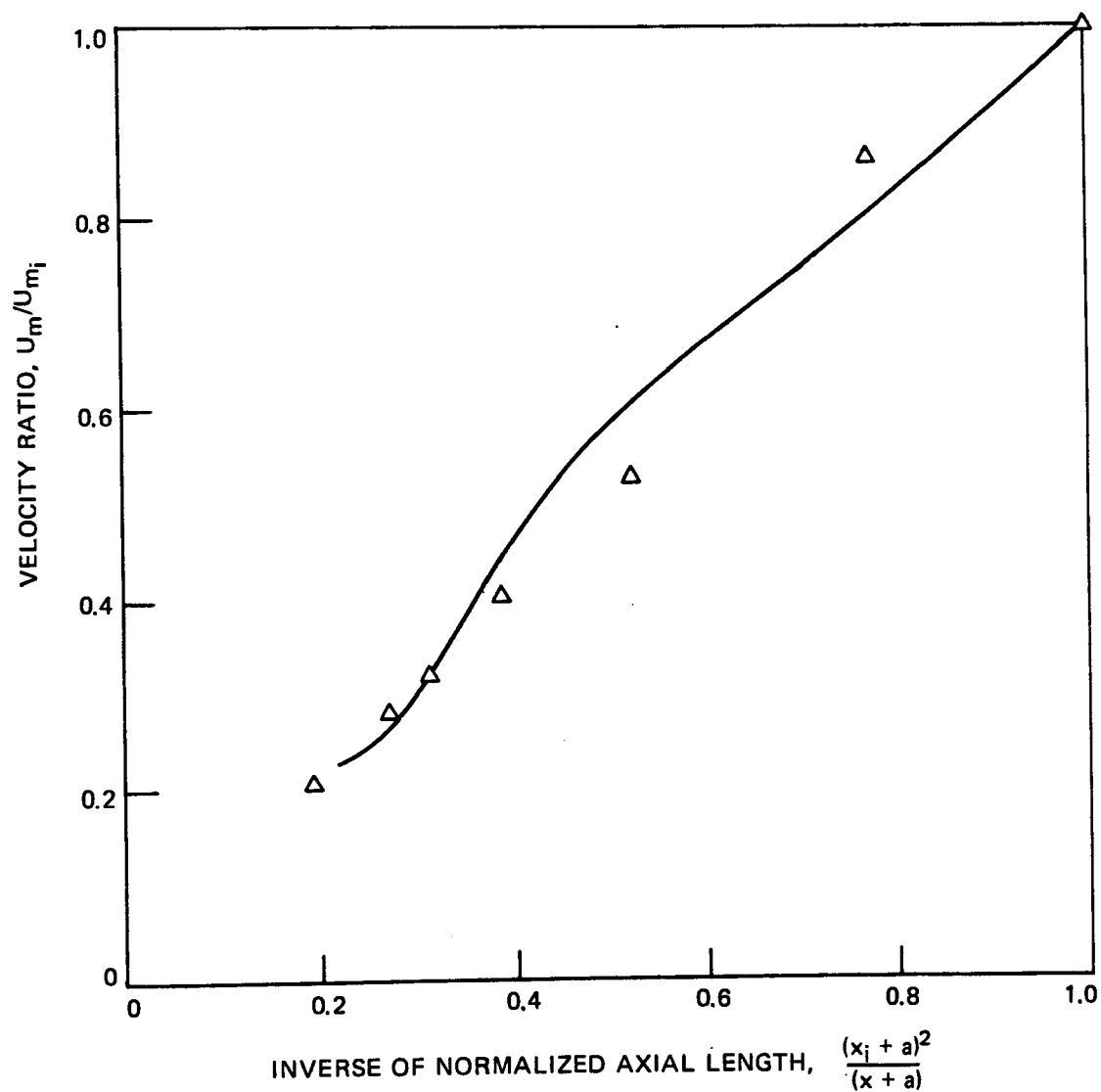


# A COMPARISON BETWEEN PREDICTED AND MEASURED AXIAL DECAY OF THE VELOCITY MAXIMUM IN A TURBULENT SWIRLING JET

INTERMEDIATELY SWIRLING JET,  $S = 0.416$

$\Delta$  MEASUREMENTS OF CHIGIER (REF. 46)

— PREDICTION

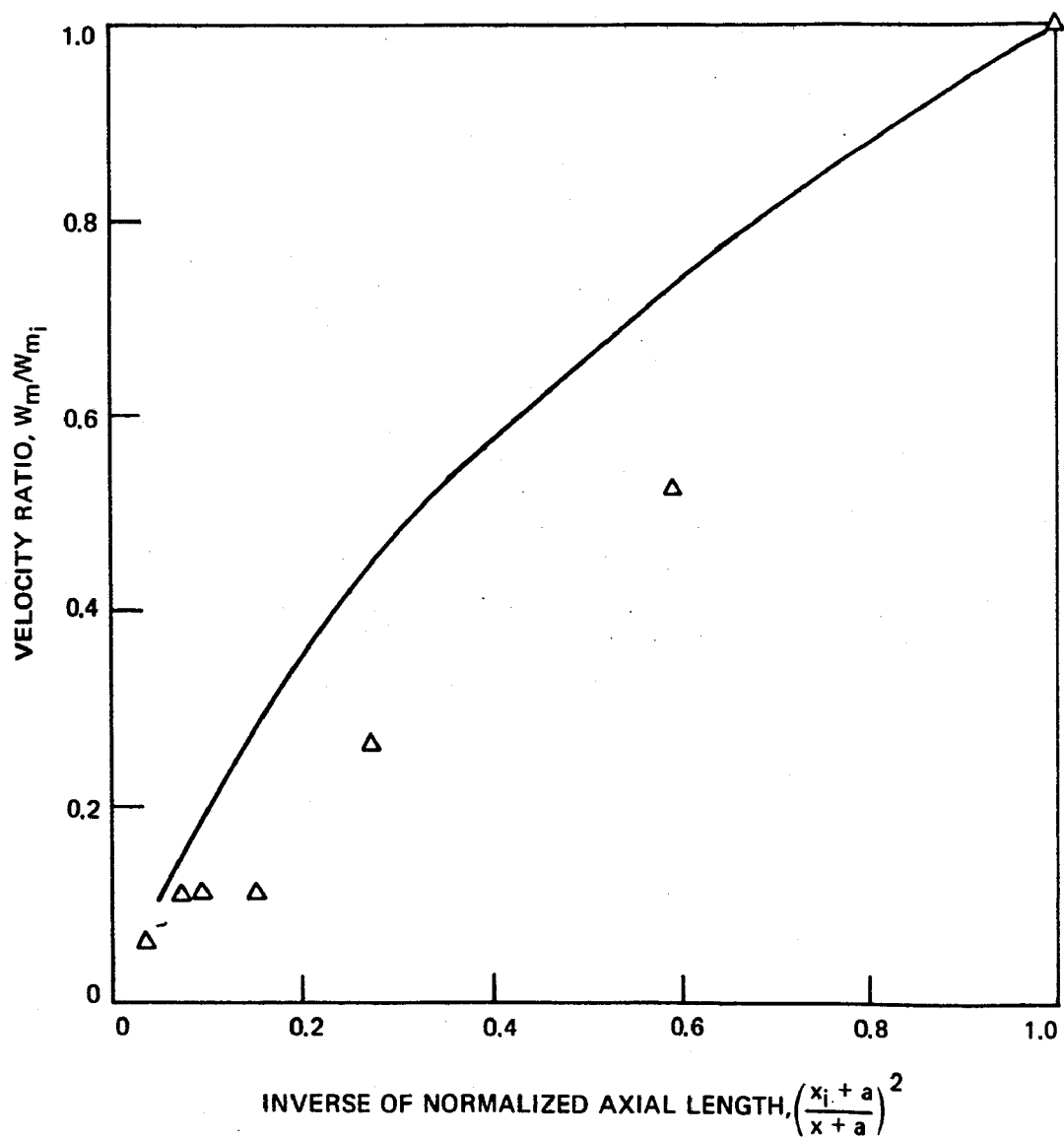


# A COMPARISON BETWEEN PREDICTED AND MEASURED AXIAL DECAY OF THE SWIRL VELOCITY MAXIMUM IN A TURBULENT SWIRLING JET

INTERMEDIATELY SWIRLING JET,  $S = 0.416$

$\Delta$  MEASUREMENTS OF CHIGIER (REF. 46)

— PREDICTION

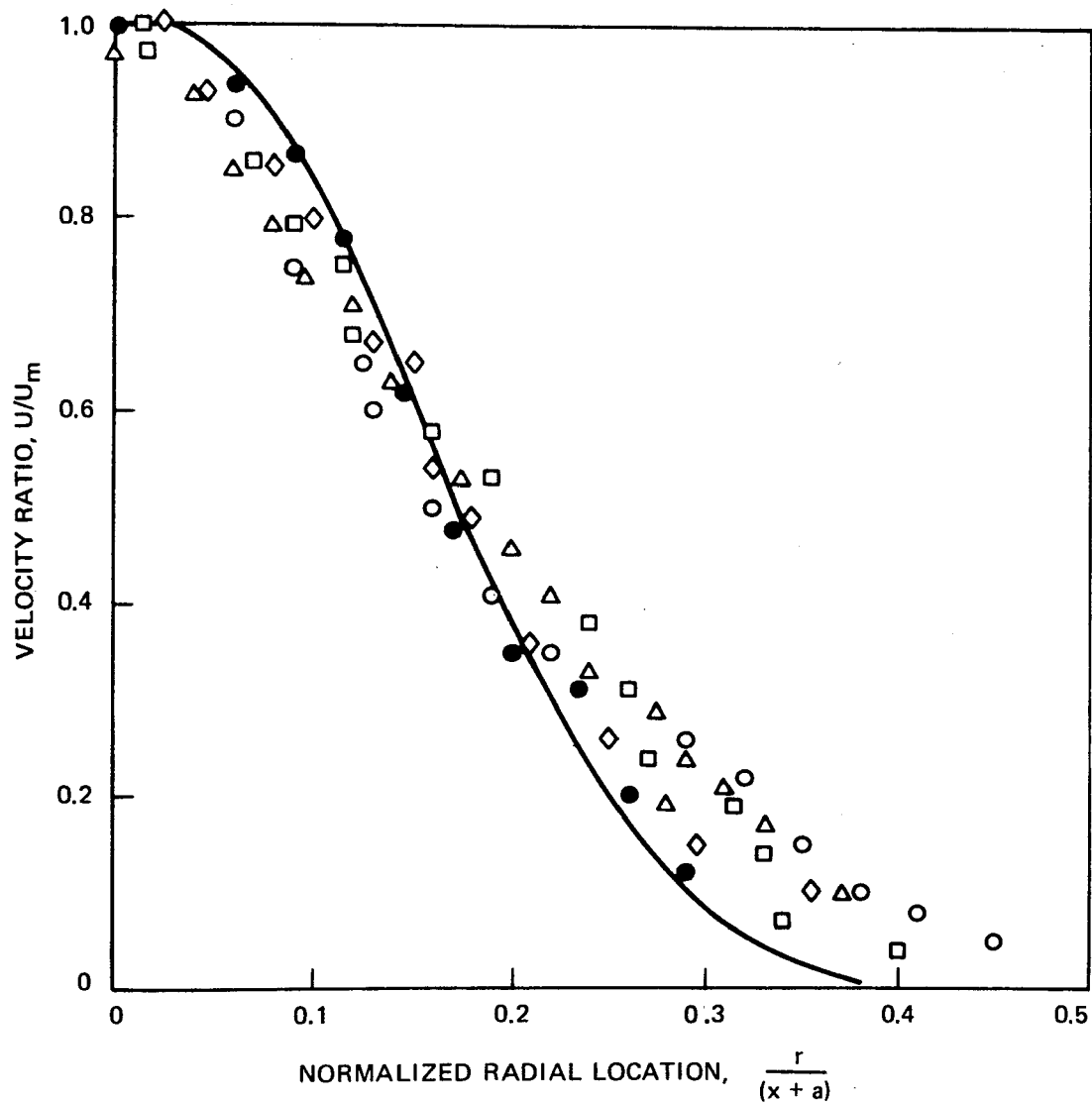


# THE COMPARISON BETWEEN THEORY AND MEASUREMENT OF THE MEAN VELOCITY PROFILE IN A TURBULENT SWIRLING JET

INTERMEDIATELY SWIRLING JET,  $S = 0.416$

○ □ △ ◇ ● MEASUREMENTS OF CHIGIER (REF. 46)

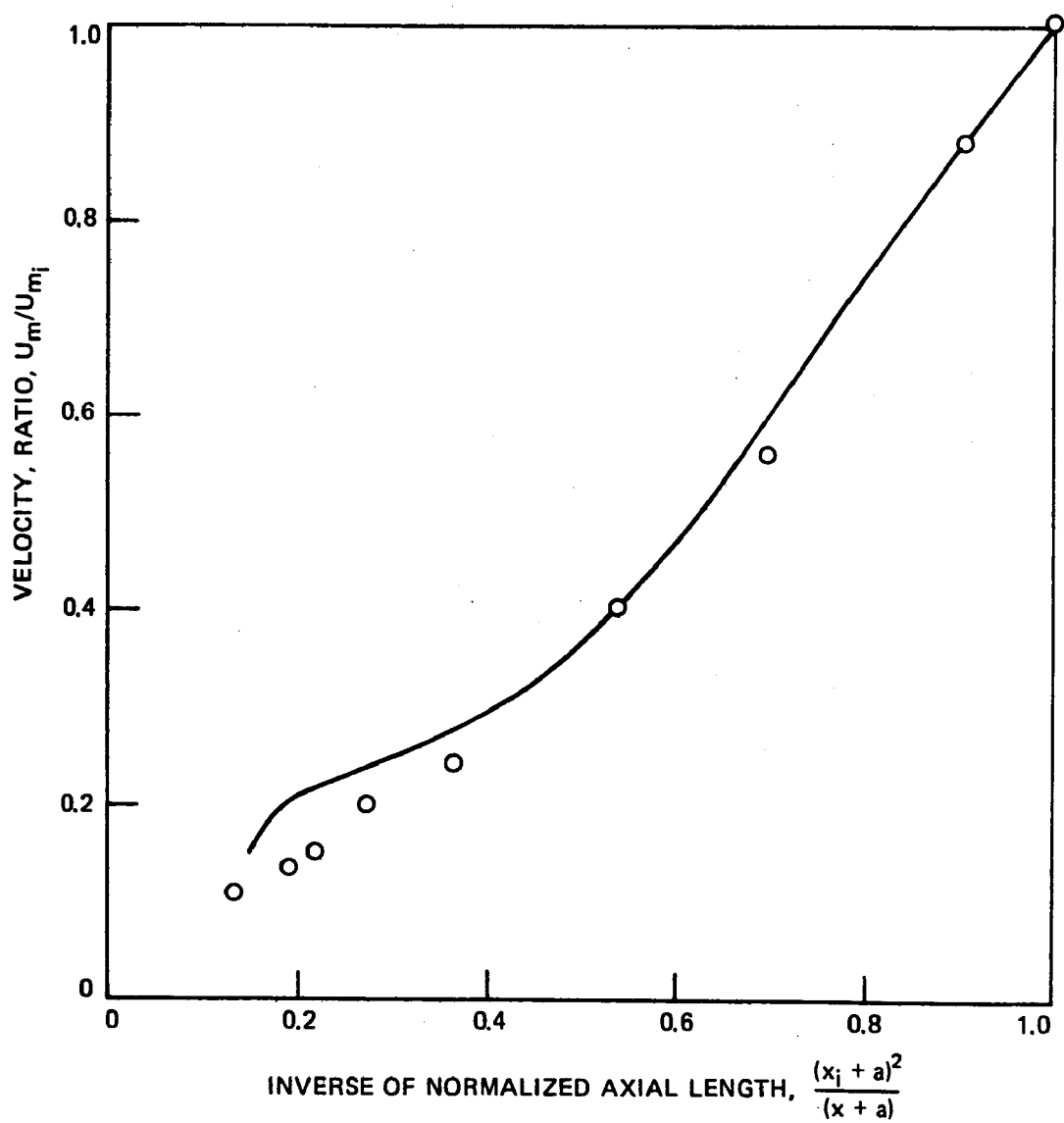
— PREDICTION



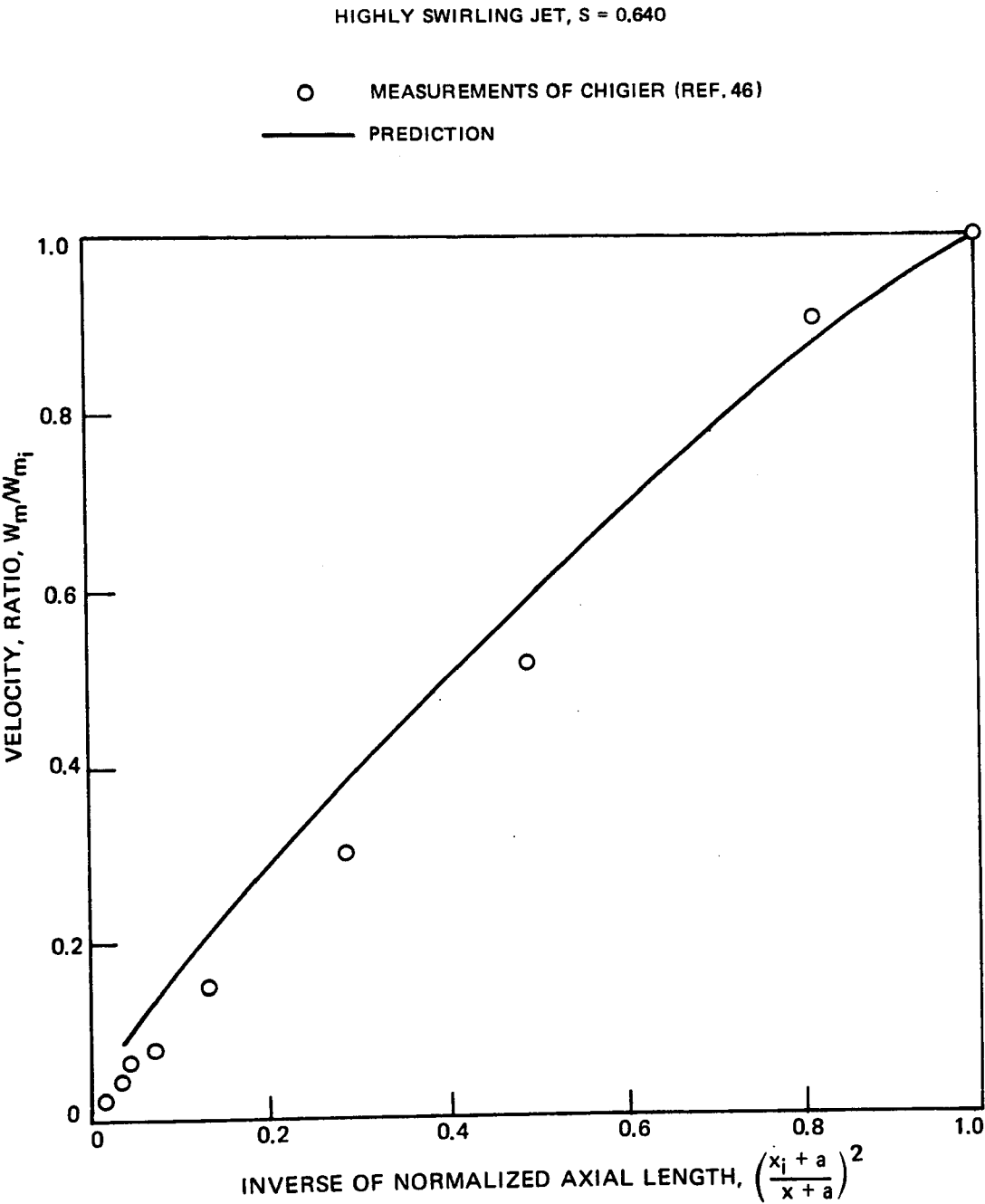
# A COMPARISON BETWEEN PREDICTED AND MEASURED AXIAL DECAY OF THE VELOCITY MAXIMUM IN A TURBULENT SWIRLING JET

HIGHLY SWIRLING JET,  $S = 0.640$

○ MEASUREMENTS OF CHIGIER (REF. 46)  
— PREDICTION



# A COMPARISON BETWEEN PREDICTED AND MEASURED AXIAL DECAY OF THE SWIRL VELOCITY MAXIMUM IN A TURBULENT SWIRLING JET



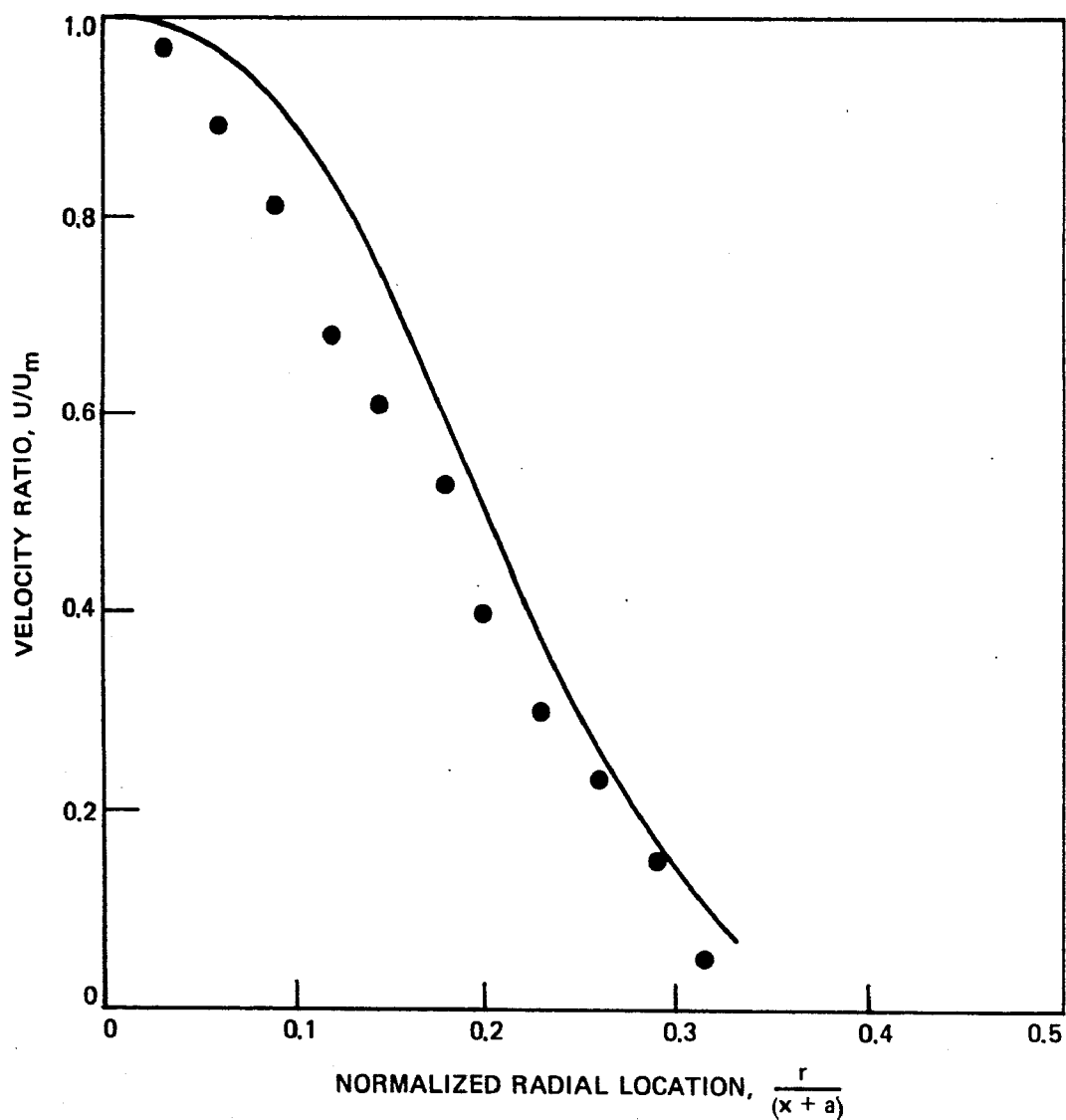


COMPARISON BETWEEN THEORY AND MEASUREMENT  
OF THE MEAN VELOCITY PROFILE IN A TURBULENT SWIRLING JET

HIGHLY SWIRLING JET,  $S = 0.640$

● MEASUREMENTS OF CHIGIER (REF. 46)

— PREDICTION



# RADIAL DISTRIBUTION OF VELOCITY VECTOR

HIGHLY SWIRLING JET,  $S = 0.600$

□ MEASUREMENTS OF CHIGIER (REF. 46)

— PREDICTION

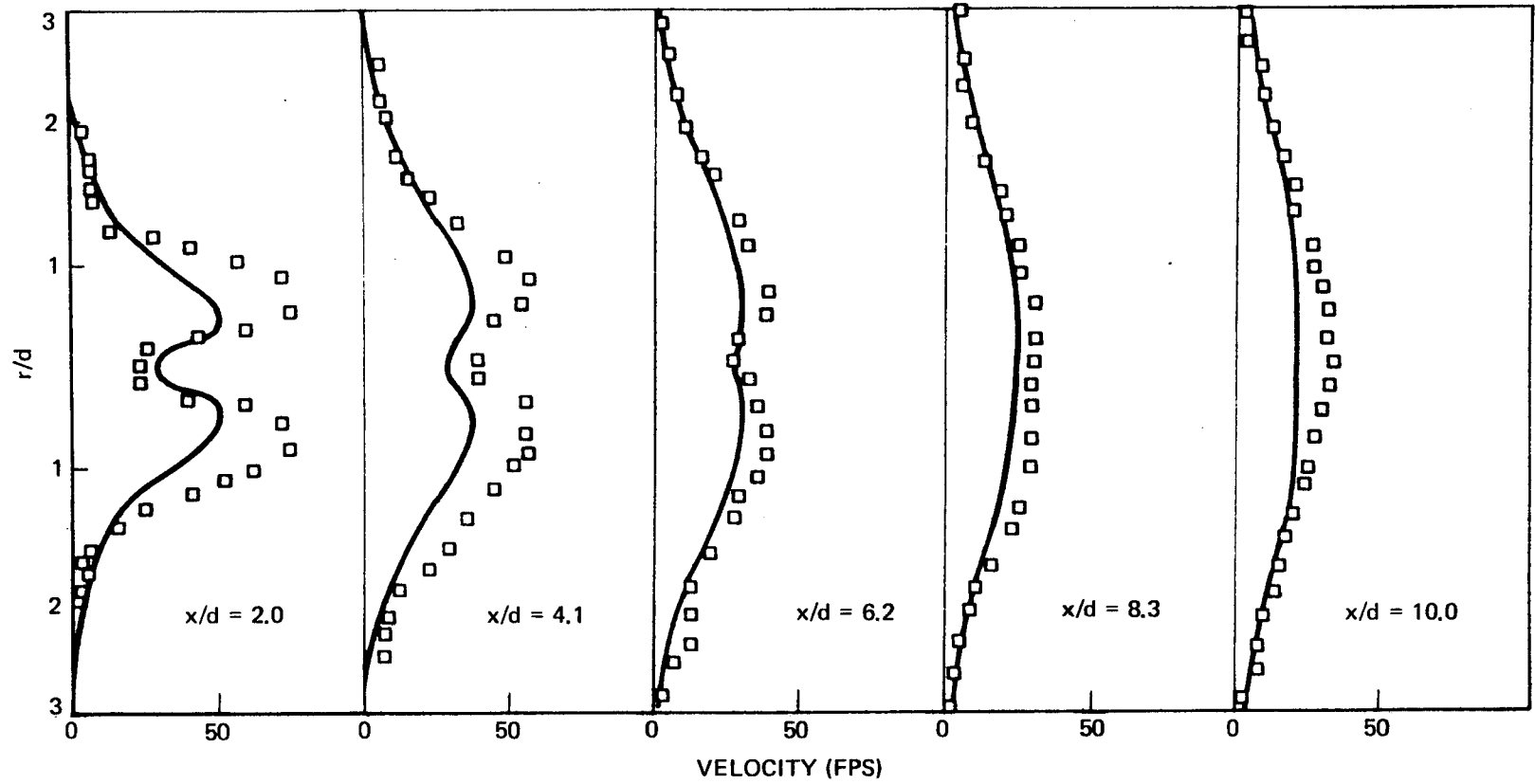


FIG. 17

# RADIAL DISTRIBUTION OF THE AXIAL VELOCITY

MINIMUM SWIRL

○ MEASUREMENTS OF LARSON ET AL (REF 47)

— PREDICTION

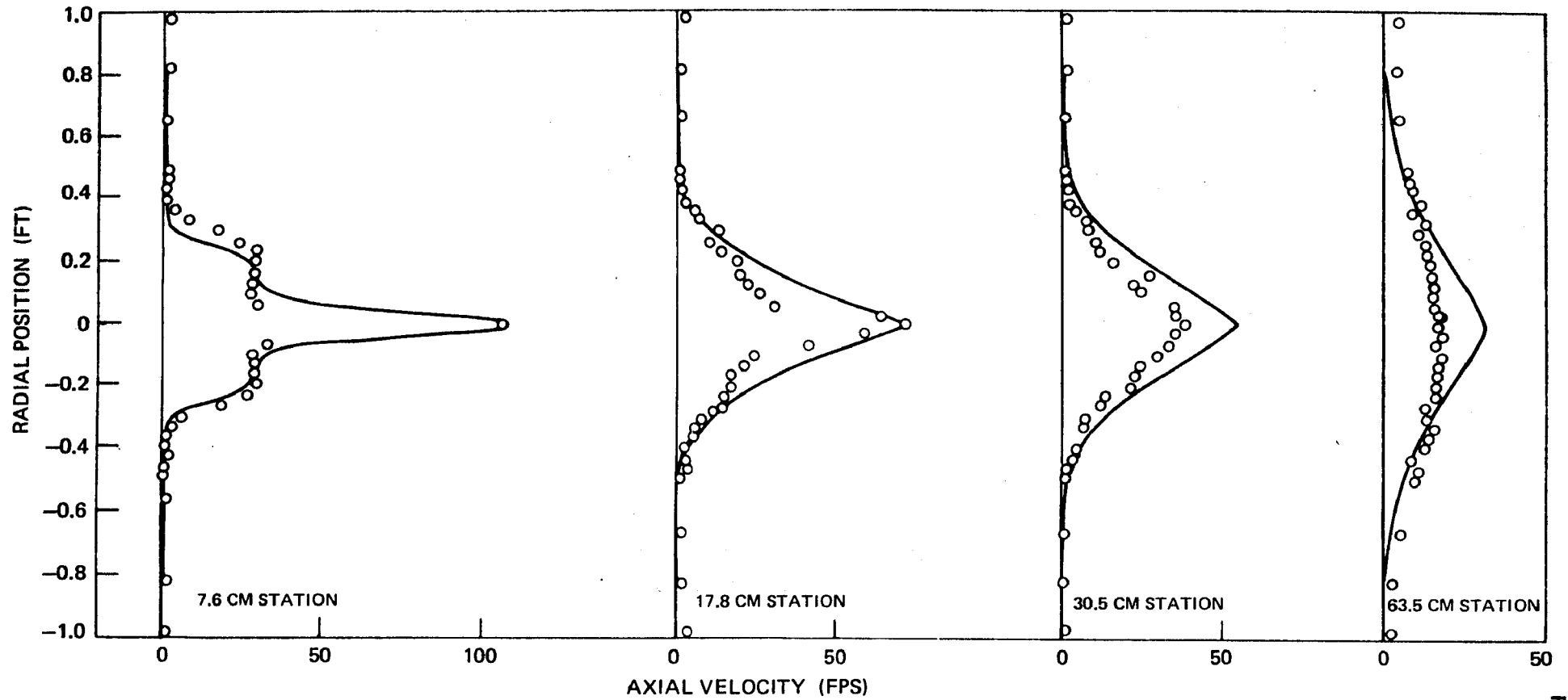


FIG.18

# RADIAL DISTRIBUTION OF AXIAL VELOCITY

HIGH SWIRL

○ MEASUREMENTS OF LARSON ET AL (REF. 47)

— PREDICTION

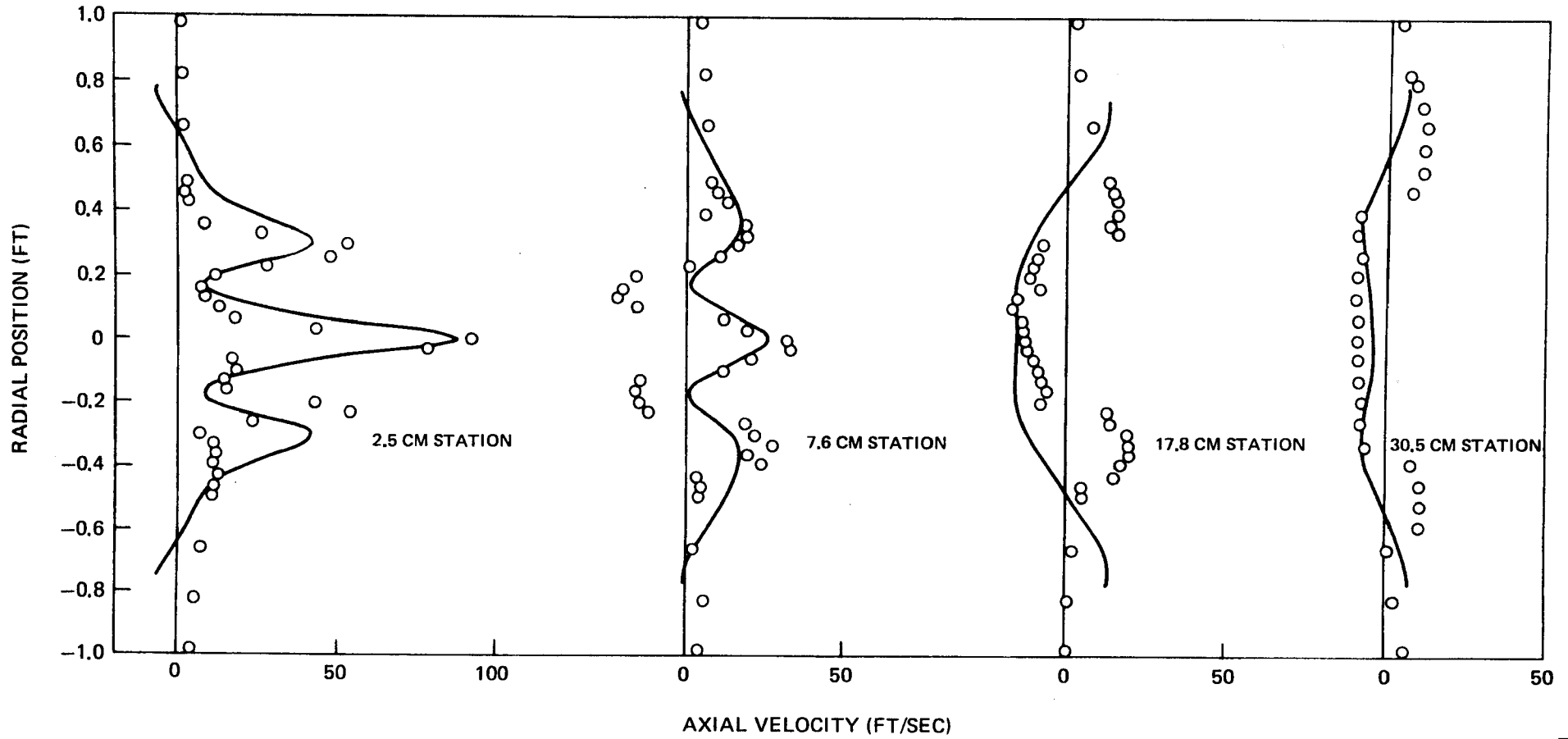


FIG. 19

THEORETICAL STREAMLINES FOR IIT SWIRL BURNER

SWIRL NUMBER = 0.8  
COLD FLOW

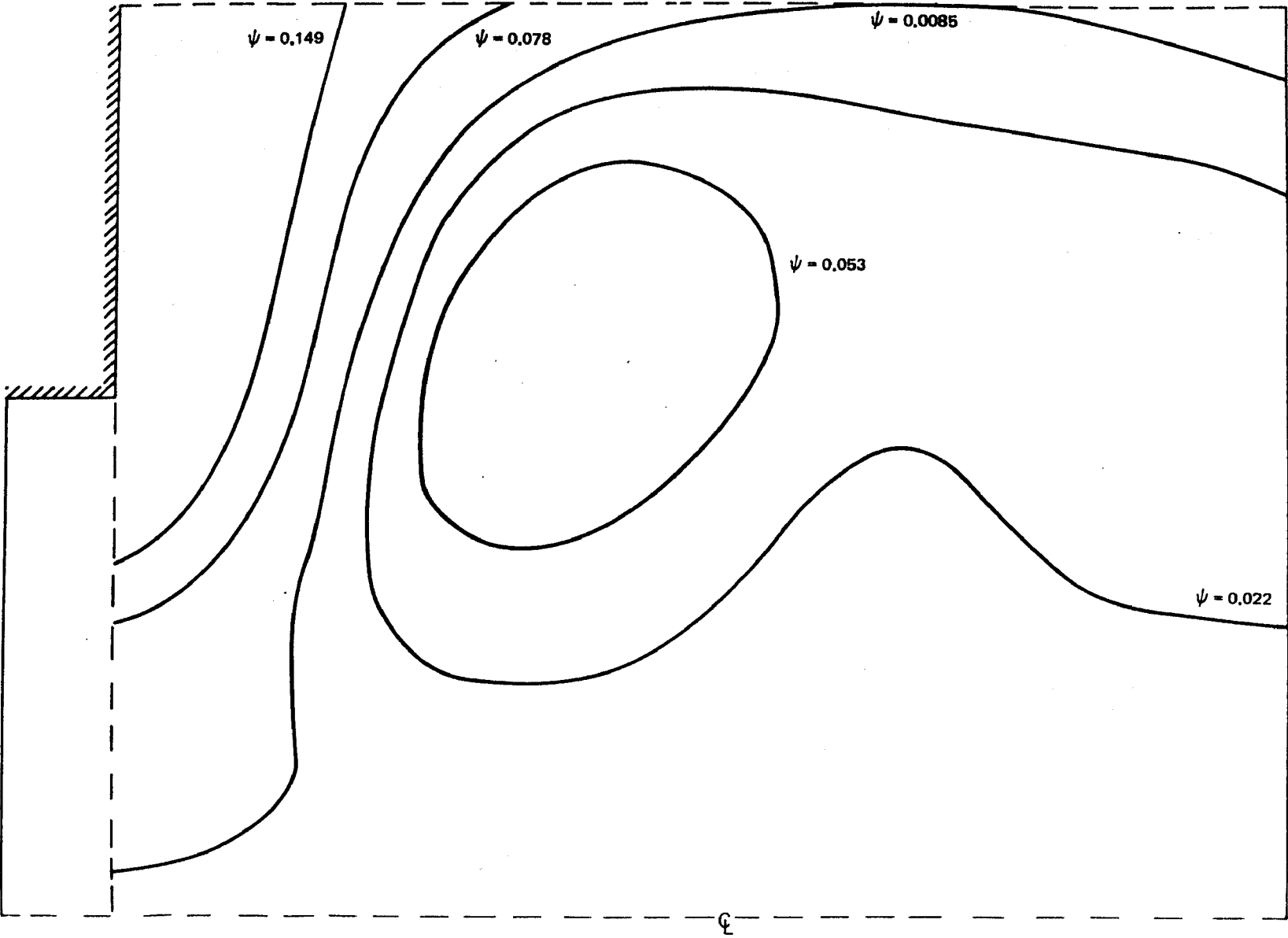


FIG. 20

Turning now to the hot flow results the predicted distributions of axial velocity are compared with the data in Fig. 21. It is immediately evident that the comparison with data is poor and that obviously the assumed inlet conditions were considerably different from those actually pertaining in the experiments. Time did not permit further (arbitrary) changes in the inlet conditions in order to better match the flow profiles at the 12.7 cms station. Evaluation of the hot flow predictive capabilities of the present procedure must, therefore, await the availability of data where the aerodynamic inlet conditions are known in detail. In Fig. 22 the predicted swirl velocities are compared with the measured data and, as in the case of the axial velocity profiles, the comparisons are poor. In particular, it is apparent that the degree of inlet swirl must have been much higher and much more localized than assumed in the calculations on the basis of the cold-flow measurements. In Fig. 23 the predicted radial profiles of temperature are compared with the data and in this case the predicted profiles are uniformly several hundred degrees Fahrenheit higher than those measured. Again, some of this discrepancy can be attributed to the unknown inlet conditions but almost certainly some of the lower measured temperatures must be the result of the energy extraction taking place at the furnace wall, and this energy extraction, for simplicity, was neglected in the present calculations. The indications are, therefore, that radiative transport was not entirely negligible, as was assumed, in performing the present calculations.

Finally, in Fig. 24, the profiles of nitric oxide are compared with the data and here, at least at the 12.7 cms station, the agreement is fair. As it happens, the agreement at the 30.5 cms location is not nearly as good and to some extent the Zeldovitch mechanism's known predisposition to under-predict nitric oxide production is balanced against the over predicted temperature levels. However, the maximum local production of nitric oxide did not exceed 10 percent of the computed equilibrium nitric oxide concentration.

In summary, little can be said of the results of the comparison with data other than it should and will be redone for some case where the inlet conditions are very carefully monitored. Finally, there is a suggestion that radiative transport effects cannot be neglected in attempting to predict pollutant levels.

**RADIAL DISTRIBUTION OF AXIAL VELOCITY**

HIGH SWIRL

○ MEASUREMENTS OF LARSON ET AL (REF. 47)

— PREDICTION

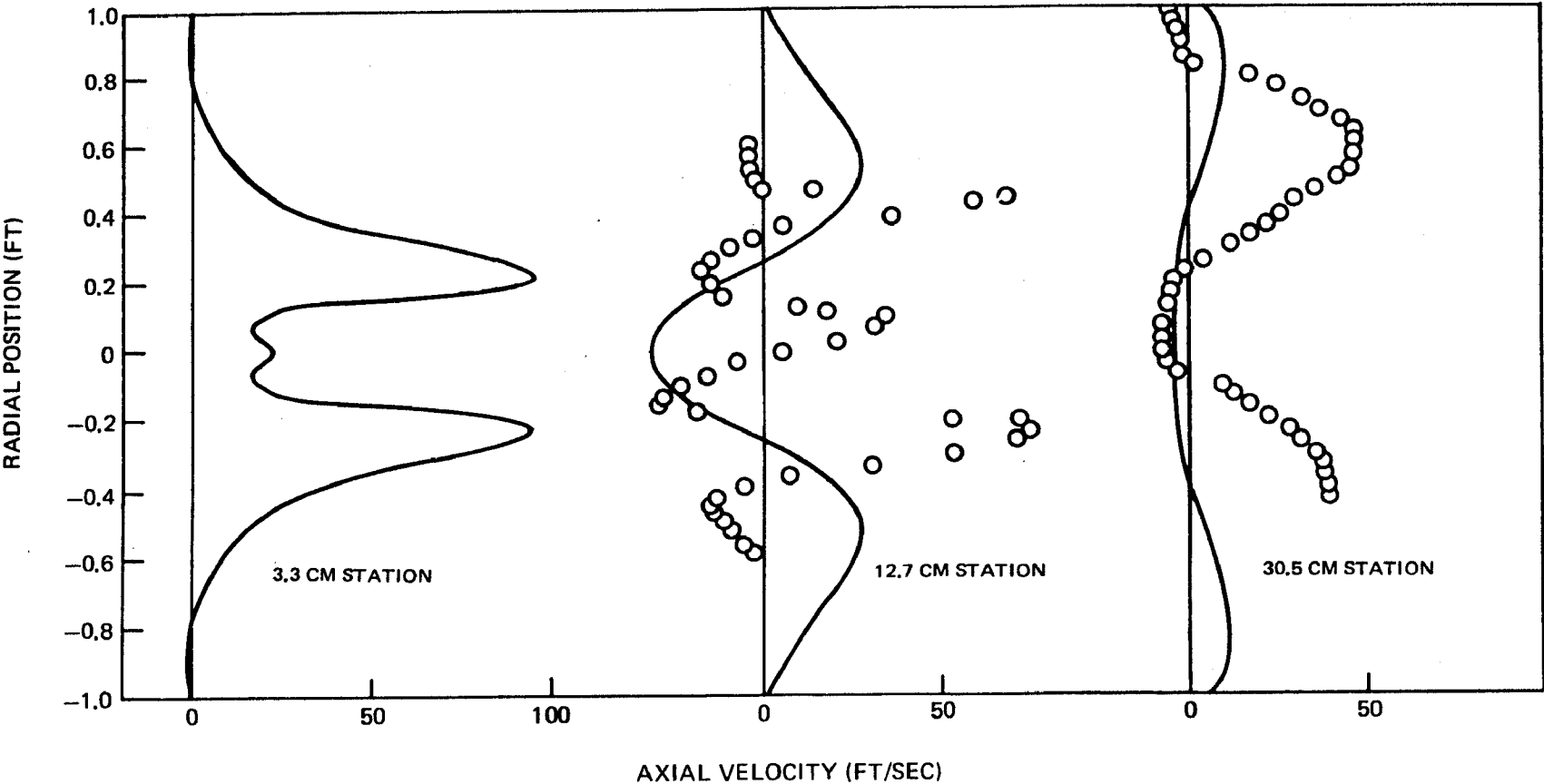


FIG. 21

# RADIAL DISTRIBUTION OF TANGENTIAL VELOCITY

HIGH SWIRL

○ MEASUREMENTS OF LARSON ET AL (REF. 47)

— PREDICTION

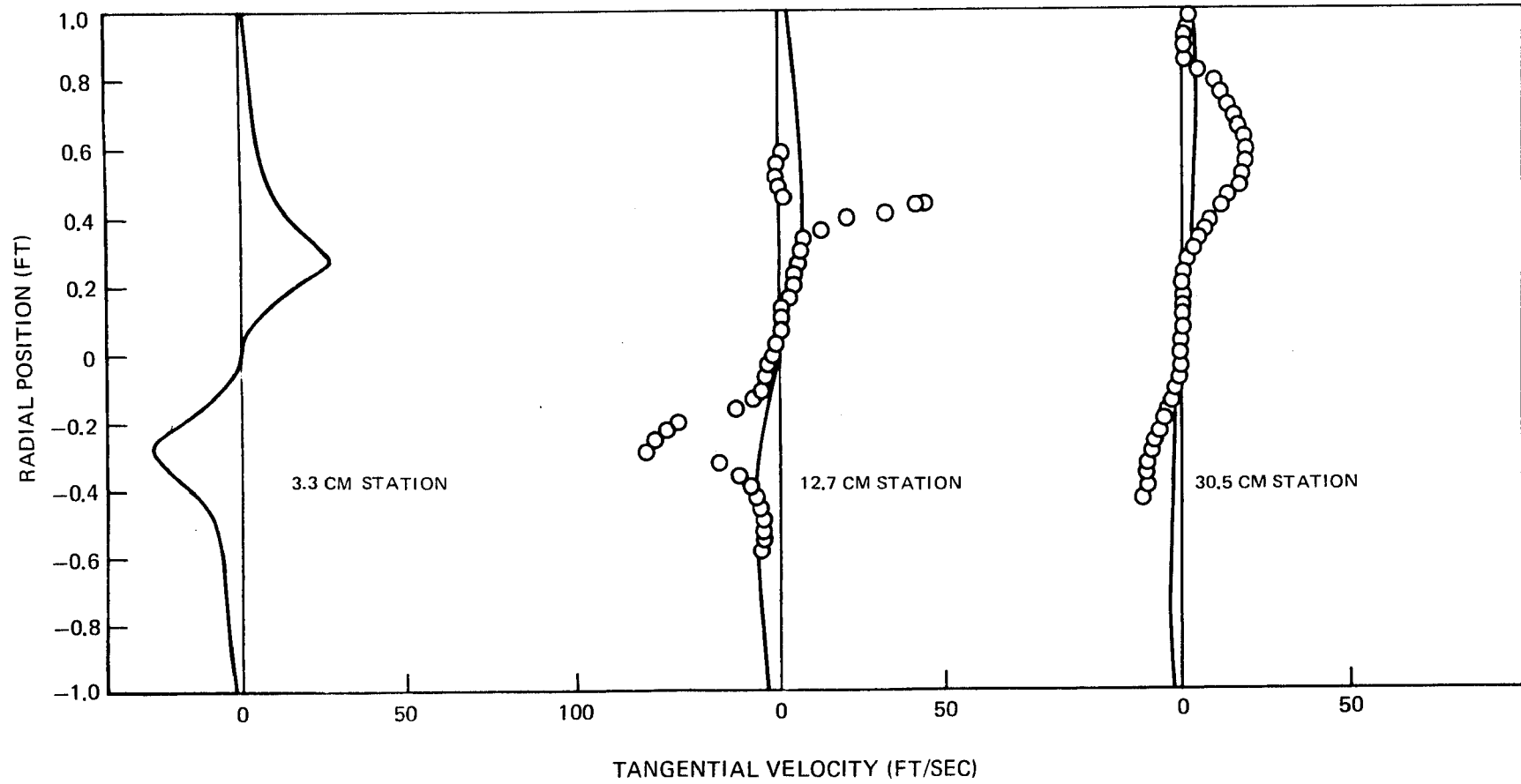


FIG. 22



# RADIAL DISTRIBUTION OF TEMPERATURE

HIGH SWIRL

○ MEASUREMENT OF LARSON ET AL (REF. 47)

— PREDICTION

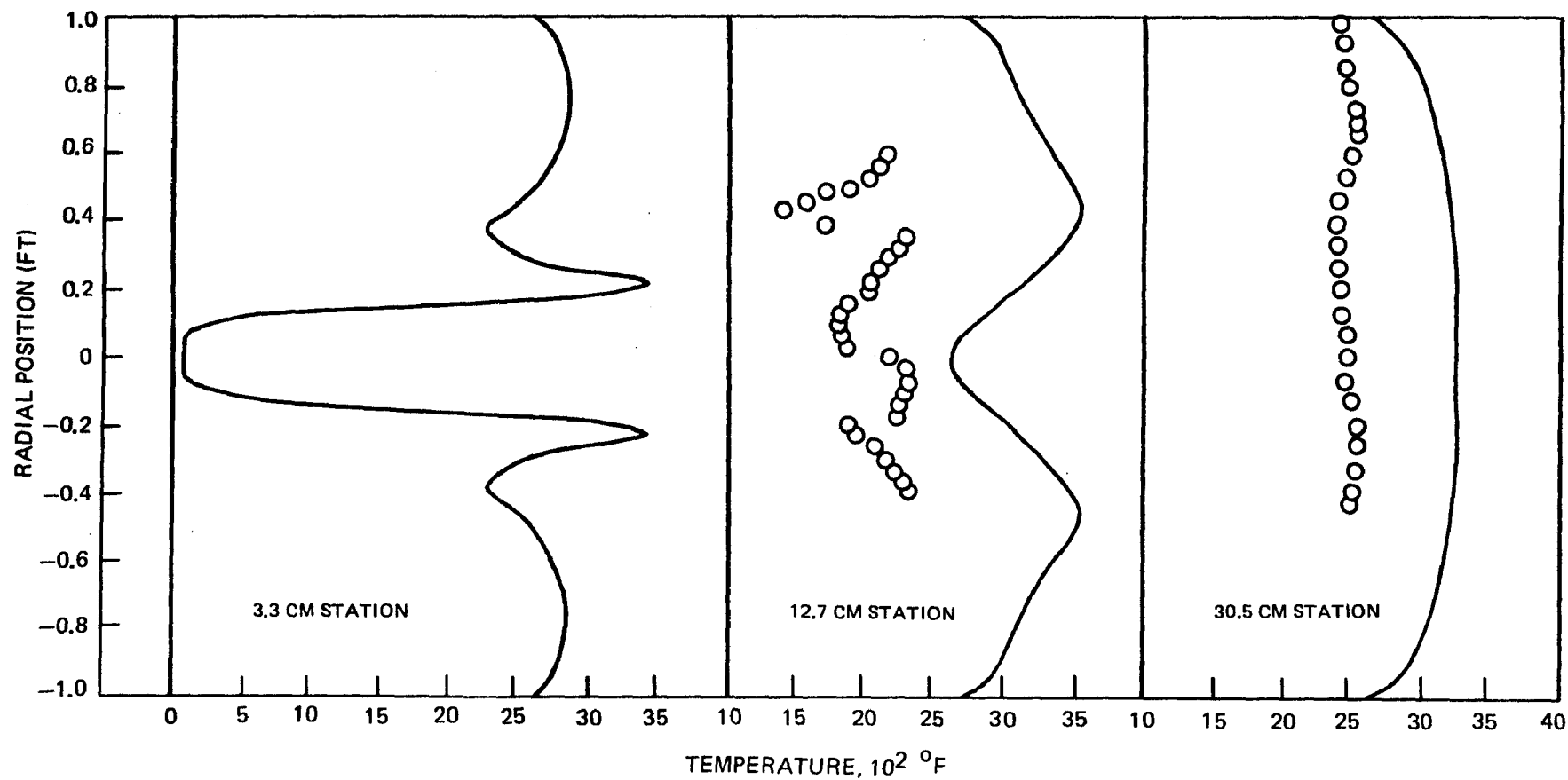


FIG. 23

RADIAL DISTRIBUTION OF NITROGEN OXIDE

HIGH SWIRL

○ MEASUREMENT OF LARSON ET AL (REF. 47)

— PREDICTION

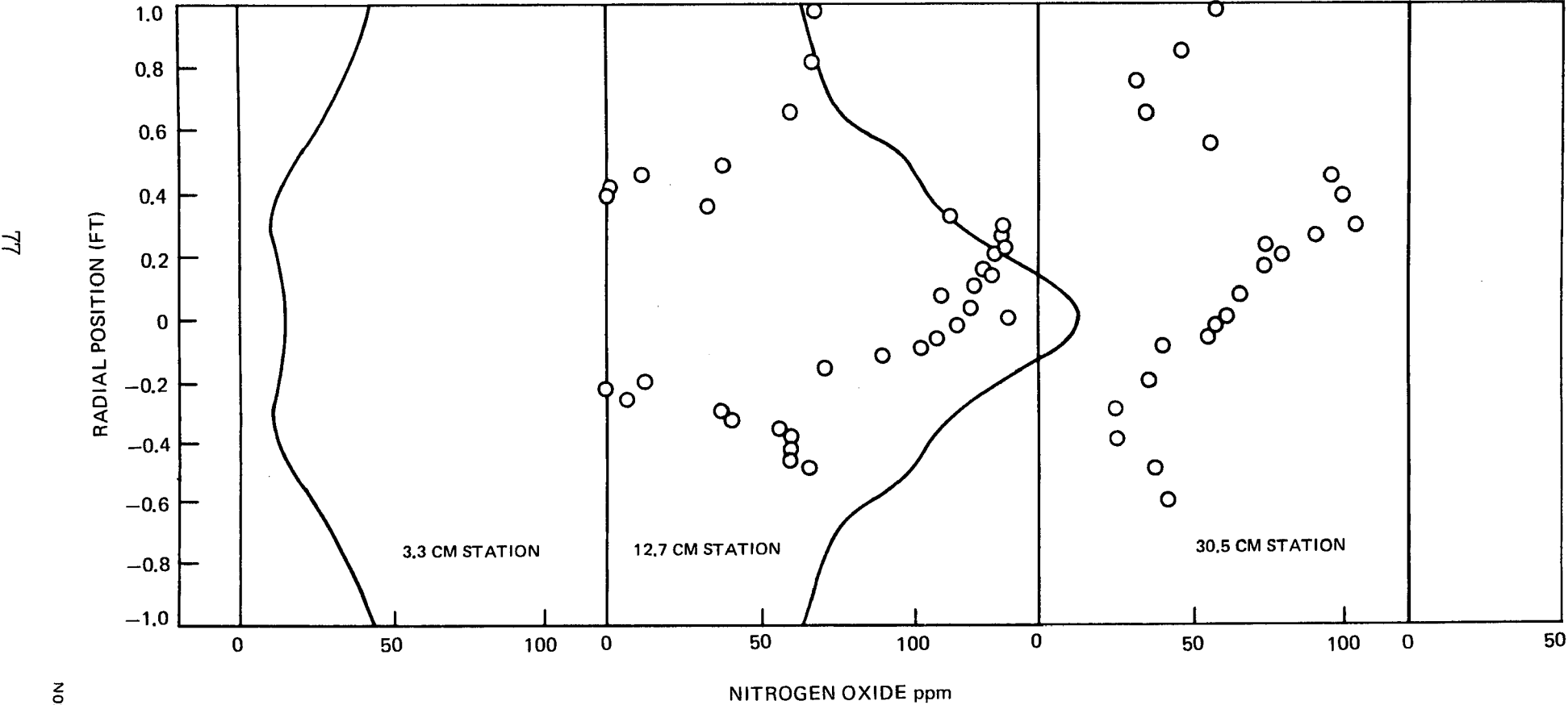


FIG. 24

## SECTION V

### CONCLUSIONS

The aim of the present study was to evaluate the predictive capability of a computational procedure for solving the time-averaged Navier-Stokes equations for the flow within a combustion device. Turbulent swirling flow with coupled chemistry and radiative heat transfer was allowed for and the following conclusions were reached:

1. Routine calculations using a novel finite-difference procedure for computing solutions of the time-averaged Navier-Stokes equations can be made for representative furnaces. Such calculations can be performed for about six hundred grid points to within a tolerance of one third of a percent in a residual for approximately ten to thirty minutes of UNIVAC 1108 computer run time, depending on the number of ancillary equations to be treated.
2. For nonreacting flows at low to moderate degrees of inlet swirl velocity very satisfactory comparisons between measured and predicted flow fields are obtained using a fairly simple turbulence model based on Prandtl's mixing length hypothesis.
3. For nonreacting flows with a high degree of inlet swirl a recirculation zone may be obtained downstream of the inlet. Even with the simple turbulence model the comparisons between measured and predicted flow fields in the region of the recirculation zone are in quite good agreement.
4. It has generally been accepted that in the recirculation zone itself that the boundary layer type of approximations are not valid, thus requiring the full Navier-Stokes equations to describe the mean flow behavior in this region. However, it seems clear from both prediction and measurement that the radial component of velocity is also large whenever the swirl velocity becomes appreciable even if a recirculation zone is not obtained. Thus the boundary layer approximations do not appear valid in flows with appreciable amounts of swirl velocity and such flows require the full Navier-Stokes equations to accurately describe the mean flow behavior.
5. For the reacting flows compared to in the present study little can be said about the predictions in view of the lack of information available on the inlet flow conditions. It can be said, however, that hot swirling flow calculations with equilibrium hydrocarbon combustion can be performed for a very acceptable computational cost employing a reasonable mesh and a fairly stringent convergence criterion by means of the UARL FREP code.

6. Highly nonlinear chemical kinetic reactions exemplified by the extended Zeldovitch mechanism for the production of nitric oxide can be incorporated into the present computational framework.

7. Although relatively untested in the present evaluation, it is felt that further improvements in the turbulence modeling, radiative transport, turbulence effect on chemical kinetics, and a better understanding of the chemical hierarchy will be required before reliable trends can be obtained by a prediction technique.

## SECTION VI

### REFERENCES

1. Beer, J. M. and N. A. Chigier: Stability and Combustion Intensity of Pulverized Coal Flames - Effect of Swirl and Impingement. Journal of the Institute of Fuel, December 1969.
2. Beer, J. M. and W. Leucker: Turbulent Flames in Rotating Flow Systems. Paper No. Inst. F-NAFTC-7, North American Fuel Technology Conference, Ottawa, Canada, 1970.
3. Beer, J. M. and J. B. Lee: The Effects of Residence Time Distribution on the Performance and Efficiency of Combustors. The Combustion Institute, 1965, pp. 1187-1202.
4. Marteney, P. J.: Analytical Study of the Kinetics of Formation of Nitrogen Oxide in Hydrocarbon - Air Combustion. Combustion Science and Technology, Vol. 1, 1970, pp. 37-45.
5. Fletcher, R. S. and J. B. Heywood: A Model for Nitric Oxide Emission from Aircraft Gas Turbine Engines. AIAA Paper 81-123, 1971.
6. Hammond, D. C. (Jr.) and A. M. Mellor: Analytical Predictions of Emissions From and Within an Allison J-33 Combustor. Combustion Science and Technology, Vol. 6, 1973, pp. 279-286.
7. Hammond, D. C. (Jr.) and A. M. Mellor: Analytical Calculations for the Performance and Pollutant Emissions of Gas Turbine Combustors. Combustion Science and Technology, Vol. 4, 1971, pp. 101-112.
8. Roberts, R., L. D. Aceto, R. Keilback, D. P. Teixeira, and J. M. Bonnell: An Analytical Model for Nitric Oxide Formation in a Gas Turbine Combustion Chamber. AIAA 9th Aerospace Sciences Meeting, Paper No. 71-715, New York, New York, 1971.
9. Mosier, S. A., R. Roberts, and R. E. Henderson: Development and Verification of an Analytical Model for Predicting Emissions from Gas Turbine Engine Combustors During Low Power Operation. 41st Meeting Propulsion and Energetics Panel of AGARD, 1973.

10. Edelman, R. and C. Economos: A Mathematical Model for Jet Engine Combustor Pollutant Emissions. AIAA Paper No. 71-714, 1971.
11. Gosman, A. D., W. M. Pun, A. K. Runchal, D. B. Spalding, and M. Wolfshtein: Heat and Mass Transfer in Recirculating Flows. Academic Press, New York, New York, 1969.
12. Anasoulis, R. F.: Computations of the Flow in a Combustor. United Aircraft Research Laboratories Report K110885-1, November 1971.
13. Bird, R. B., W. E. Stewart, and E. N. Lightfoot: Transport Phenomena. John Wiley & Sons, Inc., New York, New York, 1960.
14. Launder, B. E. and D. B. Spalding: Turbulence Models and Their Application to the Prediction of Internal Flows. Imperial College of London, Technical Engineering Department Report No. TM/TN/A/18, 1971.
15. Prandtl, L.: Bericht Uber Untersuchungen Zur Ausgebildeten Turbulenz. ZAMM, Vol. 5, 1925, p. 136.
16. Patankar, S. V. and D. B. Spalding: Heat and Mass Transfer in Boundary Layers. Intertext Books, London, England, 1970.
17. Maise, G. and H. McDonald: Mixing Length and Kinematic Eddy Viscosity in a Compressible Boundary Layer. AIAA Journal, Vol. 6, 1968, pp. 73-80.
18. McDonald, H. and F. J. Camarata: An Extended Mixing Length Approach for Computing the Turbulent Boundary Layer Development. Proceedings of the AFOSR-IFP-Stanford Conference on Boundary Layer Prediction, 1968.
19. Williamson, J. W.: An Extension of Prandtl's Mixing Length Theory. Applied Mechanics and Fluids Engineering Conference, ASME, June 1969.
20. Lilley, D. G.: Prediction of Inert Turbulent Swirl Flows. AIAA Paper No. 72-699. AIAA 5th Fluid and Plasma Dynamics Conference, June 1972.
21. Beer, J. M. and N. A. Chigier: Combustion Aerodynamics. John Wiley & Sons, Inc., New York, New York, 1972.
22. Walz, A.: Boundary Layers of Flow and Temperature. The M.I.T. Press, Cambridge, Massachusetts, 1969.

23. Lavoie, G. A., J. B. Heywood, and J. C. Keck: Experimental and Theoretical Study of Nitric Oxide Formation in Internal Combustion Engines. *Combustion Science and Technology*, Vol. 1, 1970, pp. 313-326.
24. Zeldovitch, Ya. B., P. Ya Sadounikov, and D. A. Frank-Kamenetskii: Oxidation of Nitrogen in Combustion. Academy of Sciences of USSR, Institute of Chemical Physics, Moscow-Leningrad, 1947.
25. Bowman, C. T. and D. J. Seery: Investigation of NO Formation Kinetics in Combustion Process: The Methane-Oxygen-Nitrogen Reaction, Emissions from Continuous Combustion Systems. Plenum Publishing Company, New York, New York, 1972.
26. Caretto, L. S., L. H. Muzio, R. T. Sawyer, and E. S. Starkman: The Role of Kinetics in Engine Emission of Nitric Oxide. *Combustion Sciences and Technology*, Vol. 3, 1971.
27. Baulch, D. L., D. D. Drysdale, D. G. Horne, and A. C. Lloyd: Critical Evaluation of Rate Data for Homogeneous Gas Phase Reactions of Interest in High-Temperature Systems. Report No. 4 Department of Physical Chemistry, Leeds University, United Kingdom, December 1969.
28. Campbell, I. M. and B. A. Thrush: Reactivity of Hydrogen to Atomic Nitrogen and Atomic Oxygen. *Trans. Faraday Soc.* 64, Part 5, 1968, pp. 1265-1274.
29. Brinkley, S. R.: Computational Methods in Combustion Calculations. Combustion Processes, Section C. High Speed Aerodynamics and Jet Propulsion, Vol. 2, B. Lewis, R. N. Peace, and H. S. Taylor, Eds., Princeton University, Princeton, New Jersey, 1956.
30. Brinkley, S. R.: Calculation of the Thermodynamic Properties of Multi-Component Systems and Evaluation of Propellant Performance Parameters. Proceedings of the First Conference on Kinetics, Equilibrium and Performance of High Temperature Systems, A. S. Bahn and E. E. Zukoski, Eds. The Combustion Institute, 1960, pp. 74-81.
31. Stull, D. R. and H. Prophet: Janaf Thermochemical Tables. National Bureau of Standards, U. S. Department of Commerce, NSRDS-NB537, 2nd Edition, June 1971.

32. Chen, J. C.: Simultaneous Radiative and Convective Heat Transfer in an Absorbing, Emitting and Scattering Medium in Slug Flow Between Parallel Plates. *AIChE Journal*, Vol. 10, No. 2, March 1964.
33. Viskanta, R. and R. J. Grosh: Heat Transfer by Simultaneous Conduction and Radiation in an Absorbing Medium. *Journal of Heat Transfer*, ASME, February 1962.
34. Larkin, B. K. and S. W. Churchill: Heat Transfer by Radiation Through Porous Insulations. *AIChE Journal*, Vol. 5, No. 4, December 1959.
35. Cess, R. D.: The Interaction of Thermal Radiation with Conduction and Convection Heat Transfer. *Advances in Heat Transfer*, Vol. 1, Academic Press, New York, New York, 1964.
36. Hotte, H. C. and A. F. Sarofim: Radiative Transfer. McGraw-Hill Book Company, New York, New York, 1967.
37. McAdams, W. H.: Heat Transmission. McGraw-Hill Book Company, New York, New York, 1954.
38. Hadvig, Sven: Gas Emissivity and Absorptivity: A Thermodynamic Study. *Journal of the Institute of Fuel*, April 1970, p. 129.
39. Allen, D. N. and R. V. Southwell: Relaxation Methods Applied to Determine the Motion in Two Dispersions of a Viscous Fluid Past a Fixed Cylinder. *Quarterly Journal of Mechanics and Applied Mathematics*, Vol. 8, 1955.
40. Thom, A. and C. J. Aepert: Field Computation in Engineering and Physics. D. van Nostrand Co., London, England, 1961.
41. Friedmann, M., J. Gillis, and N. Liron: Laminar Flow in a Pipe at Low and Moderate Reynolds Numbers. *Applied Scientific Research*, Vol. 19, 1968.
42. Runchal, A. K. and M. Wolfshtein: Numerical Integration Procedure for the Steady State Navier-Stokes Equations. *Journal of Mechanical Engineering Science*, Vol. 11, No. 5, 1969.
43. McDonald, J. W., V. E. Denny, and A. F. Mills: Numerical Solution of the Navier-Stokes Equations in Inlet Regions. *Journal of Applied Mechanics*, ASME, Vol. 39, No. 4, December 1972.



44. Peaceman, D. W. and H. H. Rachford, Jr.: The Numerical Solution of Parabolic and Elliptic Differential Equations. Journal of the Society of Industrial and Applied Mathematics, Vol. 3, 1965.
45. Ames, W. F.: Numerical Methods for Partial Differential Equations. Barnes & Nobels, Inc., New York, New York, 1969.
46. Chigier, N. and A. Chervinsky: Experimental and Theoretical Study of Turbulent Swirling Flow Jets Issuing From a Bound Orifice. Technion, Israel Institute of Technology, Department of Aeronautical Engineering FAE Report No. 46, November 1965.
47. Larson, D. H. and D. Shoffstall: Aerodynamic Control Over Emissions of Nitrogen Oxides and Other Pollutants From Fossil Fuel Combustion. Institute of Technology, Project No. 8933, EPA Contract No. 68-02-0216. Final Report Vol. I & II, 1973.
48. Heap, M. P. and T. M. Lowes: Development of Combustion System Design Criteria for the Control of Nitrogen Oxide Emission from Heavy Oil and Coal Furnaces. International Flame Research Foundation Ijmuiden, December 1972, EPA Contract No. 68-02-0202.

## SECTION VII

### LIST OF SYMBOLS

$A$	Frequency factor (see Eq. (37))
$a, b$	Minimum and maximum eigenvalues
$b_0, b_1, b_2$	Radiation boundary condition coefficients (see Eq. (61))
$a_\phi, b_\phi, c_\phi, d_\phi$	Coefficients in general elliptic expression, Eq. (12)
$B$	Activation energy (see Eq. (37))
$C_p$	Mean specific heat at constant pressure of mixture
$C$	Coefficients to finite difference equation
$C_x, C_y$	Generalized finite difference coefficient array
$D$	Binary diffusion coefficient
$f$	General function (see Eq. (68))
$F, G$	Radiation functions (see Eqs. (51) and (53))
$G$	Time-averaged mass velocity ( $\rho v$ ): momentum flux
$h$	Static enthalpy
$i$	Stoichiometric fuel/air ratio
$H$	Stagnation enthalpy of mixture
$I, J$	Radiation fluxes in axial direction
$i_x, i_r$	Unit vectors in $x$ and $r$ coordinate directions, respectively
$K, L$	Radiation fluxes in radial direction
$K_p$	Equilibrium constant

$k_a$	Absorption coefficient
$k_s$	Scattering coefficient
$k$	Thermal conductivity of mixture; kinetic energy of turbulent motion of mixture; rate constant
$l$	Mixing length
$L$	Heat of vaporization
$L_0$	Characteristic gas thickness (see Eq. (50))
$m$	Mass fraction; mass per unit droplet radius class: iteration parameter
$M$	Molecular weight
$n$	Normal direction
$Pr$	Effective mixture Prandtl number
$P$	Pressure
$r$	Radius: production term in species equation; droplet radius
$Q$	Heat of combustion
$Q_R$	Radiation flux
$R$	Residual: gas constant
$S$	Tangential direction
$Sc$	Effective mixture Schmidt number
$Sc_k$	Effective gaseous Schmidt number associated with turbulent kinetic energy ( $\mu_{eff}/\Gamma_k$ )
$S_x$	Swirl number (see Eq. (20))
$S_w$	Group of terms in vorticity equation (see Eq. (13))

$t$	Time
$T$	Absolute temperature
$u, v$	Velocities in $x$ and $r$ coordinate directions, respectively
$\bar{v}$	Time-averaged velocity
$w$	Swirl velocity
$x, r$	Coordinates axially and radially, respectively
$y$	Distance in radial direction
$Y_{og}$	Mass fraction of oxidant
$\epsilon$	Convergence criterion; emissivity
$\delta_{ij}$	Kronecker delta (equals unity if indices are same, or zero if different) (see also, Eq. (77))
$\Gamma_i$	Effective exchange coefficient of species $i$ ( $\rho D_i$ )
$\Gamma_h$	Effective exchange coefficient of heat ( $k/C_p$ )
$\Gamma_j$	Effective exchange coefficient of particle class ( $\rho D_j$ )
$\theta$	Circumferential direction
$\lambda$	Mixing length parameter (see Eq. (18))
$\mu$	Absolute viscosity of mixture
$\nu$	Kinematic viscosity
$\xi$	Normalized vorticity ( $\omega/r$ )
$\rho$	Density of mixture
$\sigma$	Viscosity weighting parameters (see Eq. (21)); Stephan-Boltzmann constant
$\tau$	Shear stress

$\phi$	Representative dependent variable: overall coupling and linearization term
$\psi$	Stream function
$\omega$	Vorticity

### Subscripts

eff	Imparts turbulent characteristic
g	Gas or gaseous phase
h	Upper
i	Gas phase component in mixture; grid node
j	Liquid phase component in mixture; grid node
k	Turbulent kinetic energy
l	Lower
m	Maximum
n,s	Normal and tangential direction
o	Reference
P	Particle or liquid phase
t	Tangential or swirl
w	Wall

### Superscripts

$\dagger$	Transpose of tensor
$+$	Refer to $u^+$ and $y^+$ identified in Eqs. (23) and (24)

<b>BIBLIOGRAPHIC DATA SHEET</b>	1. Report No. <b>EPA-650/2-73-045</b>	2.	3. Recipient's Accession No.
4. Title and Subtitle <b>A Study of Combustor Flow Computations and Comparison with Experiment</b>		5. Report Date <b>December 1973</b>	
7. Author(s) <b>R. F. Anasoulis and H. McDonald</b>		8. Performing Organization Rept. No.	
9. Performing Organization Name and Address <b>United Aircraft Research Laboratories 400 Main Street East Hartford, Connecticut 06108</b>		10. Project/Task/Work Unit No. <b>ROAP 21ADG-10</b>	
		11. Contract/Grant No. <b>68-02-0267</b>	
12. Sponsoring Organization Name and Address <b>EPA, Office of Research and Development NERC-RTP, Control Systems Laboratory Research Triangle Park, North Carolina 27711</b>		13. Type of Report & Period Covered <b>Final</b>	
15. Supplementary Notes		14.	
16. Abstracts The report presents a computational procedure for calculating the coupled flow and chemistry within combustion devices. The procedure solves the time-averaging Navier-Stokes equations with coupled chemistry, including the effects of turbulence and radiative heat transfer, using a novel field relaxation method. Although the procedure employs a relatively simple turbulence model, the model can be easily modified within the framework of the computational method. The flow and chemistry within a representative furnace have been computed, using the procedure; and the computations are presented and compared with experimental data.			
17. Key Words and Document Analysis. 17a. Descriptors <b>Mathematical Models Combustion Combustion Chambers Aerodynamics Navier-Stokes Equations Chemical Reactivity Turbulence Nitrogen Oxides Furnaces</b>			
17b. Identifiers/Open-Ended Terms <b>Coupled Flow Computational Procedures Radiative Heat Transfer</b>			
17c. COSATI Field/Group <b>20M, 13B</b>			
18. Availability Statement <b>Unlimited</b>		19. Security Class (This Report) <b>UNCLASSIFIED</b>	21. No. of Pages <b>94</b>
		20. Security Class (This Page) <b>UNCLASSIFIED</b>	22. Price